

From Topology to Retrieval: Decoding Embedding Spaces with Unified Signatures

Florian Rottach ^{*1,2} William Rudman ^{*3} Bastian Rieck ⁴ Harrisen Scells ¹ Carsten Eickhoff ¹

Abstract

Studying how embeddings are organized in space not only enhances model interpretability but also uncovers factors that drive downstream task performance. In this paper, we present a comprehensive analysis of topological and geometric measures across a wide set of text embedding models and datasets. We find a high degree of redundancy among these measures and observe that individual metrics often fail to sufficiently differentiate embedding spaces. Building on these insights, we introduce *Unified Topological Signatures* (UTS), a holistic framework for characterizing embedding spaces. We show that UTS can predict model-specific properties and reveal similarities driven by model architecture. Further, we demonstrate the utility of our method by linking topological structure to ranking effectiveness and accurately predicting document retrievability. We find that a holistic, multi-attribute perspective is essential to understanding and leveraging the geometry of text embeddings.

1. Introduction

Text embeddings from transformer models are central for many tasks ranging from semantic search (Zhao et al., 2024) to text classification (Da Costa et al., 2023) and clustering (Petukhova et al., 2025). They often play a crucial role in Retrieval-Augmented Generation (RAG) (Lewis et al., 2020), which combines parametric knowledge of a Large Language Model (LLM) with external knowledge from a search engine, allowing LLMs to respond with information not present in their training data. Dense retrieval models (i.e., architectures trained so that query embeddings are

highly similar to embeddings of relevant documents) are a natural choice for RAG and other information retrieval tasks due to their speed and effectiveness. Selecting the *best* model for such a task remains an open challenge. While benchmarks such as Massive Text Embedding Benchmark (MTEB) (Muennighoff et al., 2023) and theoretical frameworks (Darrin et al., 2024; Caspari et al., 2024) provide valuable tools for model comparison and selection, they do not predict or explain effectiveness on novel tasks. To gain deeper insight into representations, prior work has analyzed the geometry of word embeddings (Devlin et al., 2019) and internal representations of LLMs (Gardinazzi et al., 2024). Notably, studies have shown that effective LLM embeddings often exhibit *anisotropy* (Razzhigaev et al., 2023), with representations concentrating along a few principal axes. Additionally, evidence from the Platonic Representation Hypothesis (Huh et al., 2024) points to geometry as a key driver of model behavior, suggesting that representations from different models are converging. While these studies offer valuable insights, representational attributes are often analyzed in isolation, and text embedding models remain underexplored.

In this paper, we address this gap by analyzing the geometric and topological properties of text embedding spaces to better understand what drives model effectiveness.

Our main **contributions** are as follows:

1. A comprehensive topological analysis of text embedding spaces across a diverse set of models and retrieval datasets. We find that individual attributes fail to explain downstream effectiveness.
2. We propose *Unified Topological Signatures* (UTS), a holistic framework that combines multiple topological descriptors into a signature vector. We demonstrate that these signatures serve as distinctive fingerprints and can predict retrieval effectiveness and bias, an area not previously explored.
3. We test the Platonic Representation Hypothesis for embedding models using a novel UTS-based similarity measure. Using UTS, we find that models cluster by family, challenging the hypothesis that bigger models have convergent representations.

^{*}Equal contribution ¹University of Tübingen ²Boehringer Ingelheim GmbH, Biberach (Riss), Germany ³The University of Texas at Austin ⁴Fribourg University. Correspondence to: Florian Rottach <florian.rottach@boehringer-ingelheim.com>.

¹Preprint.

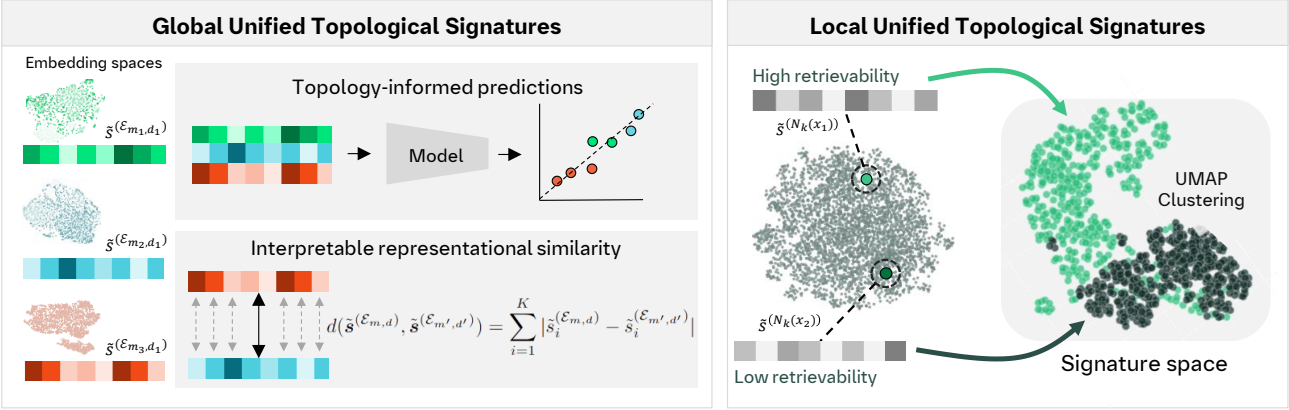


Figure 1. *Unified Topological Signatures* (UTS) for embedding spaces. **Left:** We construct signature vectors for entire embedding spaces by measuring various topological descriptors. We use the vectors for downstream prediction tasks as well as for measuring representational similarity. **Right:** We compute local signatures based on the neighborhood of individual embeddings and use them to detect retrievability bias in document corpora.

2. Related Work

Geometry of Embeddings Early studies have explored the internal representations of BERT (Devlin et al., 2019), focusing on how their geometric properties influence word senses (Reif et al., 2019). Other research has investigated isotropy (Ethayarajh, 2019), isometry (Draganov & Skiena, 2024), clustering patterns, and intrinsic dimensions (Cai et al., 2021; Torregrossa et al., 2020) of contextualized word embeddings. In evaluation studies, geometry has been identified as one of the key properties driving embedding quality (Wang et al., 2019). Recently, attention has shifted towards analyzing the internal representations of LLMs, which have been shown to be effective at many tasks without any fine-tuning (Tao et al., 2025; Gruver et al., 2024). Several works have studied the training dynamics of isotropy (Razzhigaev et al., 2023; Rudman & Eickhoff, 2024) and intrinsic dimension (Janapati & Ji, 2024; Cheng et al.; Rupnik et al., 2025), as well as the topological differences across layers (Gardinazzi et al., 2024; Liu et al., 2025). Recently, Lee et al. (2024a) found a connection between linguistic compositionality and the complexity of data manifolds. Theoretical work by Weller et al. (2025) suggests that dimensionality is a key driver for the effectiveness of embedding models. While a large body of research is focused on sentence or generally text representations, others have analyzed intrinsic dimension and other properties specifically for token embeddings (Kataiwa et al., 2025; Viswanathan et al., 2025). Notably, Lee et al. (2025a) found that token embeddings across different models share a common geometric structure. Unlike prior works examining the geometric or topological structure of embeddings, we present a *unified* framework that incorporates the full topological profile into a signature vector.

Embedding-based Retrieval Dense retrieval has emerged as a powerful alternative to traditional lexical-based retrieval methods like BM25 (Robertson et al., 2009), which are based on sparse vector representations (Zhao et al., 2024). In recent years, multiple attempts have been made to understand the geometry of embedding spaces in the context of retrieval, such as investigating the influence of local intrinsic dimension on nearest neighbor search (Aumüller & Ceccarello, 2019) and hierarchical navigable small worlds (HNSW) algorithms (Elliott & Clark, 2024). In addition, theoretical work has shown that the embedding space dimensionality is a bounding factor for retrieval effectiveness (Weller et al., 2025). However, a more complete topological perspective has not been considered for predicting retrieval effectiveness. In addition, we study the retrievability bias (Wilkie & Azzopardi, 2014a) in dense retrieval systems, which describes the phenomenon that some documents are easier to retrieve than others. Identifying such documents improves the overall retrieval quality through techniques like document augmentation (Su et al., 2025) and other optimization strategies (Setty et al., 2024). Currently, no works have attempted to link retrievability bias to geometric properties of the embedding space. We show that we can predict whether or not a document is retrievable, indicating the importance of the geometric analysis of representations of dense retrieval models.

Representational Similarity and Alignment From early work on neural pattern similarity to recent advances in cross-modal alignment in transformers, representational similarity has been central to machine learning (Sucholutsky et al., 2023). There exist a variety of methods to compare repre-

sentations, each assessing similarity with distinct aspects of granularity, symmetry, or sensitivity. In recent years, Centered Kernel Alignment (CKA) (Kornblith et al., 2019), has been widely adopted for computing similarity, mostly due to its robustness under orthogonal transformations and isotropic scaling. Caspari et al. (2024) use CKA to identify architecture as a key driver for embedding similarity, while Ciernik et al. find the objective function determining representational consistency for vision models. The similarity of representations is also at the core of the *Platonic Representation Hypothesis* (Huh et al., 2024), which argues that representations converge and foundation models become more aligned. The findings of this study indicate that the degree of alignment is shaped by the choice of similarity metric, underscoring its critical role in evaluating representational consistency. While CKA is a powerful statistical tool, it may miss topological differences in embedding spaces (Davari et al., 2022). Recent work has started to address this gap (Islam et al., 2025; Barannikov et al., 2022), but these methods focus on isolated aspects and offer little explanation for why representations diverge.

In order to provide a more holistic and interpretable view of representational similarity, we propose Unified Topological Signatures. UTS represent multidimensional profiles that summarize topology, intrinsic dimensionality, clustering behavior, and other measurable aspects of embedding spaces. In contrast to current similarity methods, we can pinpoint how embedding spaces differ. Furthermore, by looking at the global topology, we are not restricted to paired embedding spaces, which is a requirement for most local similarity measures. Finally, we examine whether the Platonic Representation Hypothesis holds under our UTS-based similarity measure, revealing new insights into the nature of this alignment.

3. Unified Topological Signatures

In this section, we define Unified Topological Signatures as multidimensional vectors that summarize embedding spaces using a diverse set of topological, geometric, and statistical descriptors. We formalize both global and local variants, outline normalization and dimensionality reduction steps, and introduce a similarity measure based on component-wise differences.

Definition Let T_i be a global descriptor of a point cloud in an n -dimensional real-valued space $X \subset \mathbb{R}^n$, where $i \in \{1, \dots, K\}$ and K is the number of descriptors. Each descriptor is a real-valued function that captures a specific topological or geometric property of the point cloud, i.e.,

$$T_i: X \rightarrow s_i^X \in \mathbb{R} \quad (1)$$

Let $\mathcal{E}_{m,d} \subset \mathbb{R}^n$ be the n -dimensional embedding space, generated by model $m \in \mathcal{M}$ on dataset $d \in \mathcal{D}$. We define

Table 1. Computed topological and geometric descriptors used for signature vectors. Mathematical and implementation details are provided in Appendix A.

MEASURE	CAT.	#SAMPLES	SOURCE
PH Dimension	Homology	5K	Adams et al. (2020)
PH Statistics	Homology	5K	Edelsbrunner et al. (2008)
Persistence Entropy	Homology	20K	Chintakunta et al. (2015)
Euler Characteristic	Homology	5K	Basu (1996)
TwoNN Dim.	Intr. Dim.	50K	Facco et al. (2017)
PCA Dim.	Intr. Dim.	50K	Fukunaga & Olsen (1971)
Effective Rank	Intr. Dim.	100K	Roy & Vetterli (2007)
Magnitude Dim.	Diversity	5K	Leinster & Willerton (2013)
Magnitude Area	Diversity	5K	Limbeck et al. (2025)
Spread	Diversity	10K	Willerton (2015)
Vendi Score	Diversity	20K	Friedman & Dieng (2022)
Pairwise Similarity	Density	50K	N/A
Uniformity	Uniformity	20K	Wang & Isola (2020)
IsoScore	Isotropy	500K	Rudman et al. (2021)
Silhouette Score	Clustering	20K	Shahapure & Nicholas (2020)

the global Unified Topological Signatures (UTS) of $\mathcal{E}_{m,d}$ as a vector:

$$\mathbf{s}^{\mathcal{E}_{m,d}} = [T_1(\mathcal{E}_{m,d}), T_2(\mathcal{E}_{m,d}), \dots, T_K(\mathcal{E}_{m,d})]^\top \quad (2)$$

where each component $s_i^{\mathcal{E}_{m,d}}$ corresponds to the value of distinct topological descriptor $T_i \in T$, with $i \in \{1, \dots, K\}$. Table 1 summarizes the selected descriptors, which cover a wide range of properties. Details and mathematical definitions for each descriptor are provided in Appendix A.

Each descriptor T_i is computed over a varying sample of n_i data points, drawn from $\mathcal{E}_{m,d}$, with n_i chosen empirically to balance descriptor robustness and computational feasibility. This ensures that each descriptor captures meaningful topological features while being computationally tractable.

Local Signatures We define a local variant of the signatures of a point $\mathbf{x} \in \mathcal{E}_{m,d}$ as:

$$\mathbf{s}^{\mathcal{N}_k(\mathbf{x})} = [T_1(\mathcal{N}_k(\mathbf{x})), \dots, T_K(\mathcal{N}_k(\mathbf{x}))]^\top \quad (3)$$

where each component $s_i^{\mathcal{N}_k(\mathbf{x})}$ corresponds to the value of T_i computed over the k -nearest neighbors of \mathbf{x} denoted by $\mathcal{N}_k(\mathbf{x}) \subset \mathcal{E}_{m,d}$.

Normalization To enable comparability across models and datasets, we normalize each signature vector computed for a point cloud X by dividing its components by the maximum absolute observed value across all embedding spaces:

$$\tilde{s}_i^X = \frac{s_i^X}{\max_{X'} |s_i^{(X')}|} \quad \text{for } i = 1, \dots, K \quad (4)$$

yielding the normalized signature vector:

$$\tilde{\mathbf{s}}^X = [\tilde{s}_1^X, \tilde{s}_2^X, \dots, \tilde{s}_K^X]^\top \quad (5)$$

Dimensionality Reduction To reduce redundancy and uncover the most informative dimensions of variation, we apply Principal Component Analysis (PCA) (Pearson, 1901) to the collection of normalized signature vectors across all embedding spaces. This yields a reduced signature:

$$\hat{s}^X = [\hat{s}_1^X, \hat{s}_2^X, \dots, \hat{s}_L^X]^\top \quad (L < K) \quad (6)$$

where each component \hat{s}_i^X is a linear combination of the original normalized descriptors, capturing the principal axes of variation in the topological feature space.

Similarity Given two normalized signature vectors $\tilde{s}^{(\mathcal{E}_{m,d})}$ and $\tilde{s}^{(\mathcal{E}_{m',d'})}$, the similarity between the corresponding embedding spaces regarding property i is quantified using the Manhattan distance:

$$\delta_i^{(\mathcal{E}_{m,d}), (\mathcal{E}_{m',d'})} = \left| \tilde{s}_i^{(\mathcal{E}_{m,d})} - \tilde{s}_i^{(\mathcal{E}_{m',d'})} \right| \quad (7)$$

These component-wise differences allow to identify which properties contribute most to the divergence between two embedding spaces. We also define an overall similarity measure as the sum of these differences:

$$d(\tilde{s}^{(\mathcal{E}_{m,d})}, \tilde{s}^{(\mathcal{E}_{m',d'})}) = \sum_{i=1}^K |\tilde{s}_i^{(\mathcal{E}_{m,d})} - \tilde{s}_i^{(\mathcal{E}_{m',d'})}| \quad (8)$$

4. Experimental Setup and Methodology

4.1. Datasets

Due to the increasing adoption of dense retrieval and its widespread applications in RAG we focus our analysis on the retrieval datasets shown in Table 2, which are included in the MTEB evaluation framework. Formally, let q denote a natural language query and d_i denote a document from a large collection $D = \{d_i\}_{i=1}^m$ consisting of m documents. Given a query, the goal of text retrieval is to return a ranked list of the n most relevant documents $L = [d_1, d_2, \dots, d_n]$ according to the relevance scores produced by a retrieval model. Dense retrieval models represent both queries and documents as dense vectors in a shared semantic space. The relevance score between a query and a document is then computed using a similarity function between their dense representations:

$$\text{Rel}(q, d) = f_{\text{sim}}(\phi_q(q), \phi_d(d))$$

where $\phi_q(\cdot)$ and $\phi_d(\cdot)$ are neural encoders mapping queries and documents into n -dimensional vectors, and f_{sim} denotes the similarity function. We conduct our experiments on 11 datasets, spanning multiple domains and corpus sizes, as detailed in Table 2.

Table 2. Retrieval datasets.

Retrieval dataset	Domain	#Queries	#Docs
MS MARCO (Nguyen et al., 2016)	Web	27	8.84M
ArguAna (Wachsmuth et al., 2018)	Argument	1406	8.67K
Touche2020 (Thakur et al., 2021)	Argument	249	528K
NFCorpus (Boteva et al., 2016)	Medical	323	3.63K
TREC-COVID (Voorhees et al., 2020)	Medical	50	171K
SciFact (Wadden et al., 2020)	Science	300	5.18K
SCIDOC5 (Cohan et al., 2020)	Science	1000	25.65K
ClimateFEVER (Diggemann et al., 2021)	Science	154	5.42M
CQADupstack (Hoogeveen et al., 2015)	Forum	1570	40.2K
QuoraRetrieval (Thakur et al., 2021)	Forum	10000	523K
FiQA2018 (Maia et al., 2018)	Finance	648	57.5K

Table 3. Embedding models.

Model	Dim.	Size	Arch.
gte-Qwen2-1.5B-instruct (Li et al., 2023)	1536	1.5B	Decoder
gte-Qwen2-7B-instruct (Li et al., 2023)	3584	7B	Decoder
stella-en-1.5B-v5 (Zhang et al., 2025a)	1024	1.5B	Decoder
Qwen3-Embedding-0.6B (Zhang et al., 2025b)	1024	0.6B	Decoder
Qwen3-Embedding-4B (Zhang et al., 2025b)	2560	4B	Decoder
Qwen3-Embedding-8B (Zhang et al., 2025b)	4096	8B	Decoder
Linq-Embed-Mistral (Kim et al., 2024)	4096	7.3B	Decoder
SFR-Embedding-Mistral (Meng et al., 2024)	4096	7.3B	Decoder
e5-mistral-7b-instruct (Wang et al., 2022)	4096	7.3B	Decoder
bge-small-en-v1.5 (Xiao et al., 2023)	384	0.02B	Encoder
bge-base-en-v1.5 (Xiao et al., 2023)	768	0.1B	Encoder
bge-large-en-v1.5 (Xiao et al., 2023)	1024	0.3B	Encoder
multilingual-e5-large-instruct (Wang et al., 2024)	1024	0.56B	Encoder
snowflake-arctic-embed-m-v1.5 (Merrick et al., 2024)	768	0.1B	Encoder
ember-v1.0 (Nur & Aliyev, 2023)	1024	0.3B	Encoder
mxbai-embed-xsmall-v1 (Lee et al., 2024b)	384	0.1B	Encoder
mxbai-embed-large-v1 (Lee et al., 2024c)	512	0.3B	Encoder
all-MiniLM-L6-v2 (Wang et al., 2020)	384	0.02B	Encoder
gtr-t5-base (Ni et al., 2021)	768	0.1B	Encoder
gtr-t5-large (Ni et al., 2021)	768	0.3B	Encoder
gtr-t5-xxl (Ni et al., 2021)	768	4.8B	Encoder
gte-small (Li et al., 2023)	384	0.3B	Encoder
gte-base (Li et al., 2023)	768	0.1B	Encoder
gte-large (Li et al., 2023)	1024	0.3B	Encoder
msmarco-roberta-ance-firsttp (Xiong et al., 2020)	768	0.1B	Encoder
msmarco-distilbert-tas-b (Hofstätter et al., 2021)	768	0.06B	Encoder
gemini-embedding-001 (Lee et al., 2025b)	3072	N/A	Decoder
openai-text-embedding-3-small (OpenAI, 2023)	1536	N/A	Decoder
openai-text-embedding-3-large (OpenAI, 2023)	3072	N/A	Decoder

4.2. Embedding models

We use 27 text embedding models from different families, including Qwen (Zhang et al., 2025b), E5 (Wang et al., 2022), T5 (Ni et al., 2021), BGE (Xiao et al., 2023) Gemini (Lee et al., 2025b) and others as listed in Table 3. The models vary in terms of size, embedding dimension, architecture, and training data. We use the models’ default text preprocessing and tokenization methods and normalize all embeddings to unit length. For each model and dataset combination, we compute embeddings for all documents and queries using MTEB. We use HuggingFace to download the open-source models (Wolf et al., 2020).

4.3. Computation of signatures

For each embedding space generated by model m on dataset d , we compute a topological signature as defined in Equation 2. Table 1 summarizes the selected descriptors, which cover a wide range of properties, including homology, intrinsic dimension, diversity, density, isotropy, and clustering. For descriptors utilizing pairwise-distances, we compute both the Euclidean and Cosine distance functions. As some methods are intractable to calculate for millions of embeddings, we perform a preliminary analysis to assess the robustness of each descriptor with respect to sample size, as discussed in Appendix B. We then sample n_i datapoints for each descriptor T_i and compute the corresponding value. To produce a larger dataset with more variability, we repeat this procedure for 3 different seeds, such that we have 891 embedding space signatures for 27 models and 11 datasets. We then normalize each signature as described above and experiment with applying PCA to reduce the dimensionality of the signatures. For the local analysis, we compute local signatures (see Equation 3) for individual documents x in the embedding space. We first compute the k -nearest neighbors of x using Cosine similarity and then compute the signature over this neighborhood following the same procedure as for the global signatures. We chose $k = 100$ to ensure the neighborhood is large enough to preserve meaningful geometric structure while remaining sufficiently local.

4.4. Topology-informed prediction models

We use the computed global signatures as feature vectors to predict 1) properties of the embedding model and 2) retrieval performance on a downstream task. We first investigate if model-specific information is encoded in the embedding space geometry. We fit a Random Forest classifier using scikit-learn (Kramer, 2016) to predict the following model properties: architecture, family, and activation function. This approach is specifically interesting for proprietary models, where such information is not publicly available. Furthermore, we study whether the signature vectors uniquely characterize embedding models by predicting the embedding model corresponding to an unseen embedding space. Lastly, we explore the relationship between topological signatures and retrieval performance. Specifically, we predict recall, mean average precision (MAP), and normalized discounted cumulative gain (NDCG) for cutoff values of $k = \{5, 20, 100\}$ directly from the model’s embedding space. The retrieval measures have been computed using MTEB (Muennighoff et al., 2023), and z-normalization is applied to make the metric scales comparable between datasets. Given the limited training data, we use 3-fold group cross-validation to predict on unseen datasets. We ensure that all data preprocessing steps are based on the training data distribution to avoid data leakage. We limit the max depth of the decision trees to 5 to prevent overfitting.

4.5. Retrievability bias detection

A document’s retrievability (Wilkie & Azzopardi, 2014a) is defined as the ease with which it can be retrieved by a given retrieval system across a set of general queries. More formally, the retrievability score $r(d)$ of a document d is defined as:

$$r(d) \propto \sum_{q \in Q} f(k_{dq}, c)$$

where Q is a set of queries, k_{dq} is the rank of document d in the retrieval results for query q , c is a cutoff rank (e.g., top-10), and $f(k_{dq}, c)$ is a function that assigns higher weights to documents appearing at higher ranks. A common choice for f is

$$f(k_{dq}, c) = \begin{cases} 1 & \text{if } d \text{ is in the top } c \text{ documents given } q, \\ 0 & \text{otherwise.} \end{cases}$$

The retrievability of a document is primarily determined by its similarity to a query. For most datasets, documents with a high query alignment (i.e., those that closely match the terms or intent of typical queries) will be more retrievable than documents that lie outside the typical query space. In dense retrieval systems documents and queries are embedded into a shared space in which similarity is influenced by the choice of embedding model. MTEB reveals that retrievability varies across embedding models despite a constant set of queries, underscoring the influence of the embedding space structure. To explore these effects in more detail, we compute the retrievability with $c = 100$ for all documents in a corpus using all available queries from the respective dataset. We then compute local signatures for the 100 most retrieved and the 100 least retrieved documents, across all combinations of models and datasets. This results in training data with 5400 samples for each of the 11 retrieval datasets. We then fit a Random Forest classifier to predict whether a document is highly retrievable, using the local UTS as feature vectors. We follow the same cross-validation strategy as for the global signatures.

Given all the retrievability scores for a specific model and dataset combination, we can also analyze the distribution of these scores to identify the overall retrievability bias of a dense retrieval system. For this, we compute the Gini coefficient (Wilkie & Azzopardi, 2014b) of the retrievability distribution and compare it to study if some models are more biased. A high Gini coefficient indicates that a small subset of documents is retrieved very frequently, while many others are rarely or never retrieved. The source code to reproduce our experiments is available at <https://github.com/Boehringer-Ingelheim/unified-topological-signatures>.

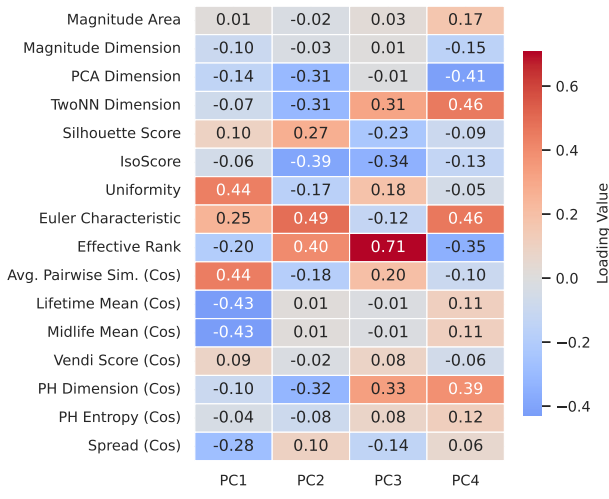


Figure 2. PCA Analysis of global UTS revealing that embedding space geometry can be summarized by only a few principal components.

5. Results

The results are organized as follows: We begin with a principal component analysis of UTS to identify key variance drivers. We then examine how UTS vectors encode model-specific features, such as architecture or activation function. Next, we show that embedding spaces cluster by model family, reflecting the influence of architecture and training data. Subsequently, we also explore the link between global UTS and retrieval performance and demonstrate the utility of local UTS in predicting document retrievability.

Global topology is summarized by a few principal components. We perform a PCA on the composition of UTS and observe that over 91% of the variance is captured by the first four principal components, as shown in Figure 2. To better understand what these components represent, we inspect the loadings of each descriptor on the principal components. We find that the first component mostly contains topological measures that are related to the pairwise distances between embeddings, including persistent homology features and kernel-based aggregations such as spread. The second component is dominated by measures related to dimensionality, isotropy, and clustering. These findings are supported by recent work establishing a connection between isotropy and clustering (Mickus et al., 2024). The remaining components contain information on various intrinsic dimension measures, as well as the effective rank. In addition to this variability analysis, we present a correlation analysis between all descriptors and model-specific properties in Appendix D. We find that many descriptors are highly correlated, indicating some redundancy in the signature.

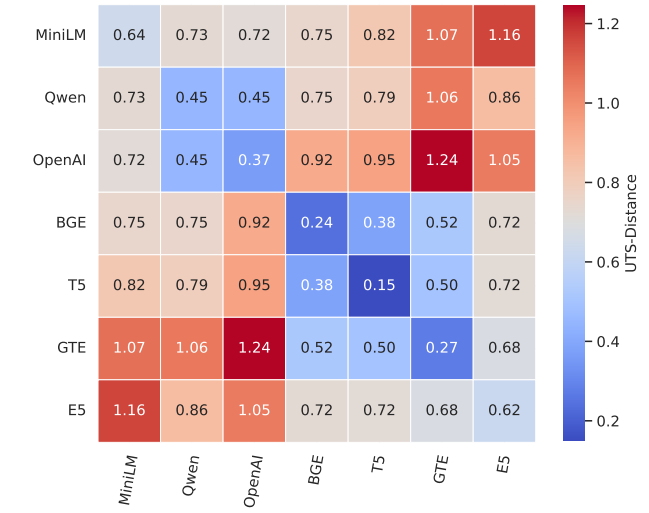


Figure 3. Model family dominates representational similarity, with lowest distances along the diagonal and clustering by architectures.

Unified Topological Signatures encode model-specific details. Table 4 summarizes the results for predicting different model attributes using the UTS as feature vectors. For unseen datasets, we can identify the specific model that generated an embedding space with a balanced accuracy of 0.55 ± 0.21 across all cross-validation folds, compared to a baseline accuracy of 0.04, which corresponds to always predicting the most frequent model among the 27 classes. Analyzing the feature importance shows that descriptors related to embedding dimension (isotropy and effective rank) are most important for identifying a model. This strong discriminative power can be attributed to the fact that the embedding dimensions are tightly linked to model architecture, with some consistently exhibiting larger dimensions. To account for this, we run the experiments separately for each embedding dimension (with sufficient data) and find that the balanced accuracy increases to 0.74 ± 0.13 for 4096 dimensions, 0.76 ± 0.23 for 1024 dimensions, 0.60 ± 0.24 for 768 dimensions and 0.64 ± 0.09 for 384 dimensions. In addition, we perform the same analysis for predicting the model family, which is an easier task with a overall balanced accuracy of 0.60 ± 0.12 . This shows that the UTS can uniquely characterize embedding models, even when controlling for embedding dimension. We discuss the prediction of architecture and activation function in Appendix G.

Global topologies cluster by model family. The Platonic Representation Hypothesis suggests that model representations converge with increasing scale. We test this by computing global UTS distances between models according to Equation 8. We average across all datasets, yielding a 27x27 distance matrix. Linkage-based hierarchical clus-

Table 4. Balanced accuracy for predicting model-specific properties from topological signatures across all folds. #Cls equals the number of classes and BL is the baseline accuracy, predicting the most frequent class.

Dataset	Model	#Cls	BL	Model family	#Cls	BL	Architecture	#Cls	BL	Activation	#Cls	BL
All	0.55 ± 0.21	27	0.04	0.60 ± 0.12	11	0.20	0.97 ± 0.02	2	0.65	0.67 ± 0.05	4	0.53
4096	0.74 ± 0.13	3	0.35	1.00 ± 0.00	2	0.70	1.00 ± 0.00	1	1.00	1.00 ± 0.00	1	1.00
1024	0.76 ± 0.23	5	0.20	0.75 ± 0.23	5	0.20	0.91 ± 0.08	2	0.80	0.92 ± 0.08	2	0.80
768	0.60 ± 0.24	8	0.13	0.74 ± 0.22	6	0.38	1.00 ± 0.00	1	1.00	0.84 ± 0.03	2	0.63
384	0.64 ± 0.09	4	0.25	0.88 ± 0.11	2	0.50	1.00 ± 0.00	1	1.00	1.00 ± 0.00	1	1.00

Table 5. Retrieval performance prediction

Metric	R2	Spearman's ρ
Recall@5	0.34 ± 0.13	0.61 ± 0.08
Recall@20	0.34 ± 0.06	0.64 ± 0.02
Recall@100	0.34 ± 0.06	0.63 ± 0.05
MAP@5	0.33 ± 0.09	0.59 ± 0.07
MAP@20	0.35 ± 0.10	0.61 ± 0.07
MAP@100	0.37 ± 0.09	0.63 ± 0.07
NDCG@5	0.36 ± 0.09	0.63 ± 0.07
NDCG@20	0.35 ± 0.09	0.62 ± 0.03
NDCG@100	0.36 ± 0.09	0.64 ± 0.03

tering (Ackerman & Ben-David, 2016) reveals that model family - not size - is the dominant factor shaping representational similarity between embedding models. To summarize this, we aggregate inter-family distances by averaging off-diagonal entries in the upper triangular part of the matrix (see Figure 3). Intra-family distances are consistently lower, indicating that architecture and training data exert stronger influence than scale. Furthermore, BERT-based models (BGE, T5, GTE) cluster tightly, as do Qwen and OpenAI models, despite size variation. These findings suggest that convergence in model representations heavily shaped by architectural choices, challenging the assumption that scaling alone drives representational convergence. In Appendix E we present additional experiments and compare our findings to similarity measured using CKA.

Retrieval performance correlates with embedding space dimensionality. We investigate how the choice of embedding model influences retrieval performance across collections, and predict different retrieval metrics using the global topology vectors. As summarized in Table 5, we find moderate correlations, suggesting that topology alone cannot fully explain retrieval performance. The best performance is achieved for Recall@20 with a mean Spearman correlation of 0.64 ± 0.02 across the cross-validation folds. As the query distribution has a strong influence on retrieval performance, we also compute the topological signature of the query embedding space and concatenate it to the signature

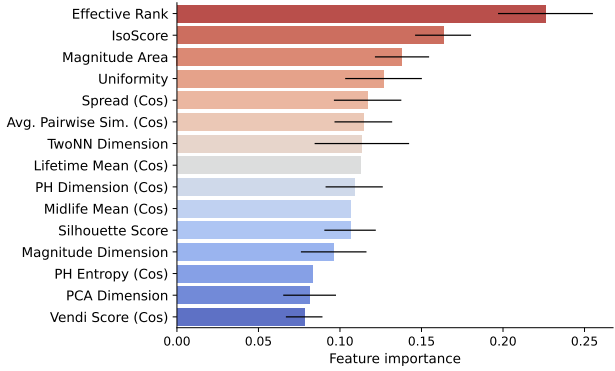


Figure 4. Feature importance for retrieval performance prediction model across all folds.

of the document embeddings. This however does not improve the performance, presumably because the queries are embedded in the same geometric space. We analyze the feature importance across all folds, summarized in Figure 4 and find that the effective rank is the most important feature. As the effective rank is highly correlated with IsoScore, we find that IsoScore is equally important when the effective rank is not included. This result is in line with recent theoretical work (Weller et al., 2025) suggesting that retrieval performance is limited by the dimensionality of the embeddings. We discuss more detailed results and additional experiments for retrieval performance prediction in Appendix F.

Local topological signatures predict document retrievability. Our analysis reveals that local UTS serve as strong predictors of document retrievability, which can be a useful approach for identifying and mitigating bias in retrieval systems. We find that highly retrievable and non-retrievable documents are well separated in the local topological signature space, as visualized in Figure 5 using UMAP (McInnes et al., 2018). We build a classifier to predict if a document is highly retrievable or not for unseen datasets, using the local UTS as feature vectors. Figure 6 summarizes the results of using signature vectors compared to baseline models that only use a single feature. Besides the local density (mean pairwise similarity), we also include local intrinsic dimen-

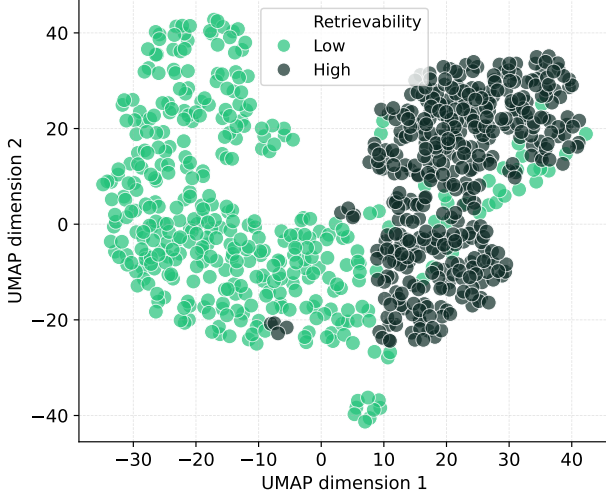


Figure 5. UMAP visualization of local UTS space for 100 highly retrievable and 100 non-retrievable documents on the QuoraRetrieval dataset.

sion as baseline, which has been found to influence retrieval (Aumüller & Ceccarello, 2019) as well as the linguistic feature word count, which has been linked to retrievability in previous studies (Wilkie & Azzopardi, 2013). In addition, we run a baseline experiment predicting retrievability directly from the raw embeddings. We find that the signature-based model achieves an average accuracy of 0.77 across all dataset cross-validation folds, significantly outperforming the baselines. This demonstrates that retrievability detection requires a holistic analysis of the local topology, beyond simple one-dimensional measures. In Appendix J, we provide additional analyses that highlight the structural differences between highly retrievable and non-retrievable documents. We also report model-specific accuracies, showing that gemini-embedding-001 is most effective for the retrievability prediction task. Finally, we investigate the overall retrievability bias of embedding models using the Gini coefficient. This analysis reveals that decoder-based models exhibit greater bias (i.e., higher inequality in document exposure), across all datasets except ArguAna.

6. Discussion and Conclusion

Discussion Our study emphasizes the importance of a holistic topological perspective on embedding spaces and reveals previously unexplored characteristics. We demonstrate that multidimensional signatures decode latent properties of embedding spaces, with feature importance distributed across descriptors. Notably, our findings challenge the assumptions of the Platonic Representation Hypothesis, indicating that further empirical investigation is needed to

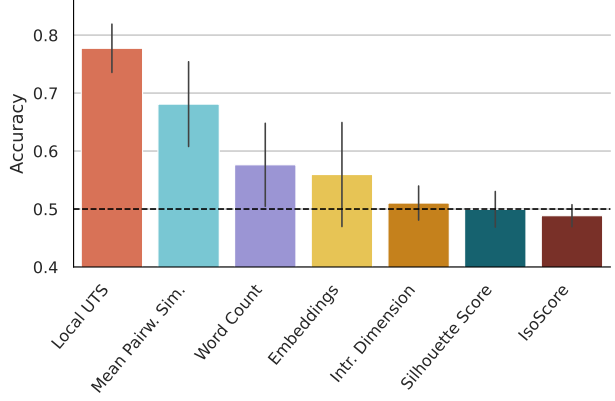


Figure 6. Cross-validation accuracy for predicting document retrievability. The dashed line indicates a random baseline.

understand how architectural choices and training data affect representational alignment. We highlight a practical application of our framework in predicting document retrievability in dense retrieval systems. This enables a targeted approach to mitigating bias, for example through document augmentation techniques, which would be impractical to apply across the entire collection.

Conclusion In this work we presented Unified Topological Signatures (UTS) to characterize the geometry of text embedding spaces. We compute a diverse set of topological and geometric descriptors for a wide range of embedding models and retrieval datasets. Our analysis reveals that models from the same family and size category share the most similar topological properties, indicating that architecture and training data have a strong influence on the embedding space geometry. Furthermore, we demonstrated that these signatures can be used to predict model properties, retrieval performance, and retrievability bias. Our findings suggest that topological signatures provide a powerful tool for understanding and optimizing text embedding spaces for retrieval tasks and beyond.

Limitations and Future work While our study sheds light on the topology of text embedding spaces, several directions for future research remain unexplored. First, the analysis of other tasks beyond retrieval, such as clustering or classification, could provide additional evidence for the relationship between topology and task performance. Second, additional studies are needed to understand how specific architectural choices and training data influence the geometry of embedding spaces. Third, scalable approximations of topological descriptors may enable more efficient analysis of large-scale embedding spaces, removing the reliance on subsampling.

References

Ackerman, M. and Ben-David, S. A characterization of linkage-based hierarchical clustering. *Journal of Machine Learning Research*, 17(231):1–17, 2016.

Adams, H., Aminian, M., Farnell, E., Kirby, M., Mirth, J., Neville, R., Peterson, C., and Shonkwiler, C. A fractal dimension for measures via persistent homology. In *Topological Data Analysis: The Abel Symposium 2018*, pp. 1–31. Springer, 2020.

Aumüller, M. and Ceccarello, M. The role of local intrinsic dimensionality in benchmarking nearest neighbor search. In *International Conference on Similarity Search and Applications*, pp. 113–127. Springer, 2019.

Bac, J., Mirkes, E. M., Gorban, A. N., Tyukin, I., and Zinov'yev, A. Scikit-dimension: a python package for intrinsic dimension estimation. *Entropy*, 23(10):1368, 2021.

Barannikov, S., Trofimov, I., Balabin, N., and Burnaev, E. Representation topology divergence: A method for comparing neural network representations, 2022. URL <https://arxiv.org/abs/2201.00058>.

Basu, S. On bounding the betti numbers and computing the euler characteristic of semi-algebraic sets. In *Proceedings of the twenty-eighth annual ACM symposium on Theory of computing*, pp. 408–417, 1996.

Bauer, U. Ripser: efficient computation of Vietoris-Rips persistence barcodes. *J. Appl. Comput. Topol.*, 5(3):391–423, 2021. ISSN 2367-1726. doi: 10.1007/s41468-021-00071-5. URL <https://doi.org/10.1007/s41468-021-00071-5>.

Boteva, V., Gholipour, D., Sokolov, A., and Riezler, S. A full-text learning to rank dataset for medical information retrieval. 2016. URL <http://www.cl.uni-heidelberg.de/~riezler/publications/papers/ECIR2016.pdf>.

Cai, X., Huang, J., Bian, Y., and Church, K. Isotropy in the contextual embedding space: Clusters and manifolds. In *International conference on learning representations*, 2021.

Caspari, L., Dastidar, K. G., Zerhoudi, S., Mitrovic, J., and Granitzer, M. Beyond benchmarks: Evaluating embedding model similarity for retrieval augmented generation systems. *arXiv preprint arXiv:2407.08275*, 2024.

Cheng, E., Doimo, D., Kervadec, C., Macocco, I., Yu, J., Laio, A., and Baroni, M. Emergence of a high-dimensional abstraction phase in language transformers, 2024. URL <https://arxiv.org/abs/2405.15471>. *Model GRIDE k OPT-125m*, 64.

Chintakunta, H., Gentimis, T., Gonzalez-Diaz, R., Jimenez, M.-J., and Krim, H. An entropy-based persistence barcode. *Pattern Recognition*, 48(2):391–401, 2015.

Ciernik, L., Linhardt, L., Morik, M., Dippel, J., Kornblith, S., and Muttenthaler, L. Objective drives the consistency of representational similarity across datasets. In *Forty-second International Conference on Machine Learning*.

Cohan, A., Feldman, S., Beltagy, I., Downey, D., and Weld, D. S. Specter: Document-level representation learning using citation-informed transformers, 2020. URL <https://arxiv.org/abs/2004.07180>.

Da Costa, L. S., Oliveira, I. L., and Fileto, R. Text classification using embeddings: a survey. *Knowledge and Information Systems*, 65(7):2761–2803, 2023.

Darrin, M., Formont, P., Ayed, I., Cheung, J. C., and Piantanida, P. When is an embedding model more promising than another? *Advances in Neural Information Processing Systems*, 37:68330–68379, 2024.

Davari, M., Horoi, S., Natik, A., Lajoie, G., Wolf, G., and Belilovsky, E. Reliability of cka as a similarity measure in deep learning. *arXiv preprint arXiv:2210.16156*, 2022.

Devlin, J., Chang, M.-W., Lee, K., and Toutanova, K. Bert: Pre-training of deep bidirectional transformers for language understanding. In *Proceedings of the 2019 conference of the North American chapter of the association for computational linguistics: human language technologies, volume 1 (long and short papers)*, pp. 4171–4186, 2019.

Diggelmann, T., Boyd-Graber, J., Bulian, J., Ciaramita, M., and Leippold, M. Climate-fever: A dataset for verification of real-world climate claims, 2021.

Draganov, O. and Skiena, S. The shape of word embeddings: Quantifying non-isometry with topological data analysis. In *Findings of the Association for Computational Linguistics: EMNLP 2024*, pp. 12080–12099. Association for Computational Linguistics, 2024. doi: 10.18653/v1/2024.findings-emnlp.705. URL <http://dx.doi.org/10.18653/v1/2024.findings-emnlp.705>.

Edelsbrunner, H., Harer, J., et al. Persistent homology—a survey. *Contemporary mathematics*, 453(26):257–282, 2008.

Elliott, O. P. and Clark, J. The impacts of data, ordering, and intrinsic dimensionality on recall in hierarchical navigable small worlds. In *Proceedings of the 2024 ACM SIGIR International Conference on Theory of Information Retrieval*, pp. 25–33, 2024.

Ethayarajh, K. How contextual are contextualized word representations? comparing the geometry of bert, elmo,

and gpt-2 embeddings. *arXiv preprint arXiv:1909.00512*, 2019.

Facco, E., d’Errico, M., Rodriguez, A., and Laio, A. Estimating the intrinsic dimension of datasets by a minimal neighborhood information. *Scientific reports*, 7(1):12140, 2017.

Friedman, D. and Dieng, A. B. The vendi score: A diversity evaluation metric for machine learning. *arXiv preprint arXiv:2210.02410*, 2022.

Fukunaga, K. and Olsen, D. R. An algorithm for finding intrinsic dimensionality of data. *IEEE Transactions on computers*, 100(2):176–183, 1971.

Gardinazzi, Y., Viswanathan, K., Panerai, G., Ansuini, A., Cazzaniga, A., and Biagetti, M. Persistent topological features in large language models. *arXiv preprint arXiv:2410.11042*, 2024.

Gruver, N., Finzi, M., Qiu, S., and Wilson, A. G. Large language models are zero-shot time series forecasters, 2024. URL <https://arxiv.org/abs/2310.07820>.

Gupta, A., Ozdemir, A., and Anumanchipalli, G. Geometric interpretation of layer normalization and a comparative analysis with rmsnorm. *arXiv preprint arXiv:2409.12951*, 2024.

Hofstätter, S., Lin, S.-C., Yang, J.-H., Lin, J., and Hanbury, A. Efficiently Teaching an Effective Dense Retriever with Balanced Topic Aware Sampling. In *Proc. of SIGIR*, 2021.

Hoogeveen, D., Verspoor, K. M., and Baldwin, T. Cquadupstack: A benchmark data set for community question-answering research. In *Proceedings of the 20th Australasian document computing symposium*, pp. 1–8, 2015.

Huh, M., Cheung, B., Wang, T., and Isola, P. The platonic representation hypothesis. *arXiv preprint arXiv:2405.07987*, 2024.

Islam, M. T., Liu, D., and Sarkar, D. Manifold approximation leads to robust kernel alignment, 2025. URL <https://arxiv.org/abs/2510.22953>.

Janapati, S. and Ji, Y. A comparative study of learning paradigms in large language models via intrinsic dimension. *arXiv preprint arXiv:2412.06245*, 2024.

Kataiwa, T., Hakaze, C., and Ohki, T. Measuring intrinsic dimension of token embeddings. *arXiv preprint arXiv:2503.02142*, 2025.

Kim, J., Lee, S., Kwon, J., Gu, S., Kim, Y., Cho, M., yong Sohn, J., and Choi, C. Linq-embed-mistral: Elevating text retrieval with improved gpt data through task-specific control and quality refinement. <https://getling.com/blog/ling-embed-mistral/>, 2024. Linq AI Research Blog.

Kornblith, S., Norouzi, M., Lee, H., and Hinton, G. Similarity of neural network representations revisited. In *International conference on machine learning*, pp. 3519–3529. PMIR, 2019.

Kramer, O. Scikit-learn. In *Machine learning for evolution strategies*, pp. 45–53. Springer, 2016.

Lee, A., Weber, M., Viégas, F., and Wattenberg, M. Shared global and local geometry of language model embeddings. *arXiv preprint arXiv:2503.21073*, 2025a.

Lee, J., Chen, F., Dua, S., Cer, D., Shanbhogue, M., Naim, I., Ábrego, G. H., Li, Z., Chen, K., Vera, H. S., Ren, X., Zhang, S., Salz, D., Boratko, M., Han, J., Chen, B., Huang, S., Rao, V., Suganthan, P., Han, F., Doumanoglou, A., Gupta, N., Moiseev, F., Yip, C., Jain, A., Baumgartner, S., Shahi, S., Gomez, F. P., Mariserla, S., Choi, M., Shah, P., Goenka, S., Chen, K., Xia, Y., Chen, K., Duddu, S. M. K., Chen, Y., Walker, T., Zhou, W., Ghiya, R., Gleicher, Z., Gill, K., Dong, Z., Seyedhosseini, M., Sung, Y., Hoffmann, R., and Duerig, T. Gemini embedding: Generalizable embeddings from gemini, 2025b. URL <https://arxiv.org/abs/2503.07891>.

Lee, J. H., Jiralerspong, T., Yu, L., Bengio, Y., and Cheng, E. Geometric signatures of compositionality across a language model’s lifetime. *arXiv preprint arXiv:2410.01444*, 2024a.

Lee, S., Lipp, J., Huang, R., and Koenig, D. Every byte matters: Introducing mxbai-embed-xsmall-v1, 2024b. URL <https://www.mixedbread.ai/blog/mxbai-embed-xsmall-v1>.

Lee, S., Shakir, A., Koenig, D., and Lipp, J. Open source strikes bread - new fluffy embeddings model, 2024c. URL <https://www.mixedbread.ai/blog/mxbai-embed-large-v1>.

Leinster, T. and Willerton, S. On the asymptotic magnitude of subsets of euclidean space. *Geometriae Dedicata*, 164(1):287–310, 2013.

Lewis, P., Perez, E., Piktus, A., Petroni, F., Karpukhin, V., Goyal, N., Küttler, H., Lewis, M., Yih, W.-t., Rocktäschel, T., et al. Retrieval-augmented generation for knowledge-intensive nlp tasks. *Advances in neural information processing systems*, 33:9459–9474, 2020.

Li, Z., Zhang, X., Zhang, Y., Long, D., Xie, P., and Zhang, M. Towards general text embeddings with multi-stage contrastive learning. *arXiv preprint arXiv:2308.03281*, 2023.

Limbeck, K. and Simons, E. Magnipy: A python library for computing magnitude of metric spaces. <https://github.com/aidos-lab/magnipy>, 2025. GitHub repository.

Limbeck, K., Andreeva, R., Sarkar, R., and Rieck, B. Metric space magnitude for evaluating the diversity of latent representations, 2025. URL <https://arxiv.org/abs/2311.16054>.

Liu, X., Hsiung, L., Yang, Y., and Yan, Y. Spectral insights into data-oblivious critical layers in large language models. *arXiv preprint arXiv:2506.00382*, 2025.

Maia, M., Handschuh, S., Freitas, A., Davis, B., McDermott, R., Zarrouk, M., et al. Financial opinion mining and question answering. URL: <https://sites.google.com/view/fiqa/home>, 2018.

McInnes, L., Healy, J., and Melville, J. Umap: Uniform manifold approximation and projection for dimension reduction. *arXiv preprint arXiv:1802.03426*, 2018.

Meng, R., Liu, Y., Joty, S. R., Xiong, C., Zhou, Y., and Yavuz, S. Sfr-embedding-mistral: Enhance text retrieval with transfer learning. <https://www.salesforce.com/blog/sfr-embedding/>, 2024. Salesforce AI Research Blog.

Merrick, L., Xu, D., Nuti, G., and Campos, D. Arctic-embed: Scalable, efficient, and accurate text embedding models. *arXiv preprint arXiv:2405.05374*, 2024.

Mickus, T., Grönroos, S.-A., and Attieh, J. Isotropy, clusters, and classifiers. *arXiv preprint arXiv:2402.03191*, 2024.

Muennighoff, N., Tazi, N., Magne, L., and Reimers, N. Mteb: Massive text embedding benchmark, 2023. URL <https://arxiv.org/abs/2210.07316>.

Nguyen, T., Rosenberg, M., Song, X., Gao, J., Tiwary, S., Majumder, R., and Deng, L. Ms marco: A human-generated machine reading comprehension dataset. 2016.

Ni, J., Qu, C., Lu, J., Dai, Z., Ábrego, G. H., Ma, J., Zhao, V. Y., Luan, Y., Hall, K. B., Chang, M.-W., and Yang, Y. Large dual encoders are generalizable retrievers, 2021. URL <https://arxiv.org/abs/2112.07899>.

Nur, E. and Aliyev, A. ember-v1: Sota embedding model, 2023.

OpenAI. New embedding models and api updates. <https://openai.com/index/new-embedding-models-and-api-updates/>, 2023. Accessed: 2025-11-10.

Pearson, K. On lines and planes of closest fit to systems of points in space. *Philosophical Magazine*, 2(11):559–572, 1901.

Petukhova, A., Matos-Carvalho, J. P., and Fachada, N. Text clustering with large language model embeddings. *International Journal of Cognitive Computing in Engineering*, 6:100–108, 2025.

Razhigaev, A., Mikhalkuk, M., Goncharova, E., Osledets, I., Dimitrov, D., and Kuznetsov, A. The shape of learning: Anisotropy and intrinsic dimensions in transformer-based models. *arXiv preprint arXiv:2311.05928*, 2023.

Reif, E., Yuan, A., Wattenberg, M., Viegas, F. B., Coenen, A., Pearce, A., and Kim, B. Visualizing and measuring the geometry of bert. *Advances in neural information processing systems*, 32, 2019.

Reimers, N. and Gurevych, I. The curse of dense low-dimensional information retrieval for large index sizes. In *Proceedings of the 59th Annual Meeting of the Association for Computational Linguistics and the 11th International Joint Conference on Natural Language Processing (Volume 2: Short Papers)*, pp. 605–611, 2021.

Robertson, S., Zaragoza, H., et al. The probabilistic relevance framework: Bm25 and beyond. *Foundations and Trends® in Information Retrieval*, 3(4):333–389, 2009.

Roy, O. and Vetterli, M. The effective rank: A measure of effective dimensionality. In *2007 15th European signal processing conference*, pp. 606–610. IEEE, 2007.

Rudman, W. and Eickhoff, C. Stable anisotropic regularization, 2024. URL <https://arxiv.org/abs/2305.19358>.

Rudman, W., Gillman, N., Rayne, T., and Eickhoff, C. Isoscore: Measuring the uniformity of embedding space utilization. *arXiv preprint arXiv:2108.07344*, 2021.

Ruppik, B. M., von Rohrscheidt, J., van Niekerk, C., Heck, M., Vukovic, R., Feng, S., Lin, H.-c., Lubis, N., Rieck, B., Zibrowius, M., et al. Less is more: Local intrinsic dimensions of contextual language models. *arXiv preprint arXiv:2506.01034*, 2025.

Setty, S., Thakkar, H., Lee, A., Chung, E., and Vidra, N. Improving retrieval for rag based question answering models on financial documents, 2024. URL <https://arxiv.org/abs/2404.07221>.

Shahapure, K. R. and Nicholas, C. Cluster quality analysis using silhouette score. In *2020 IEEE 7th international conference on data science and advanced analytics (DSAA)*, pp. 747–748. IEEE, 2020.

Su, W., Tang, Y., Ai, Q., Yan, J., Wang, C., Wang, H., Ye, Z., Zhou, Y., and Liu, Y. Parametric retrieval augmented generation, 2025. URL <https://arxiv.org/abs/2501.15915>.

Sucholutsky, I., Muttenthaler, L., Weller, A., Peng, A., Bobu, A., Kim, B., Love, B. C., Grant, E., Groen, I., Achterberg, J., et al. Getting aligned on representational alignment. *arXiv preprint arXiv:2310.13018*, 2023.

Tao, C., Shen, T., Gao, S., Zhang, J., Li, Z., Hua, K., Hu, W., Tao, Z., and Ma, S. Llms are also effective embedding models: An in-depth overview, 2025. URL <https://arxiv.org/abs/2412.12591>.

Thakur, N., Reimers, N., Rücklé, A., Srivastava, A., and Gurevych, I. BEIR: A heterogeneous benchmark for zero-shot evaluation of information retrieval models. In *Thirty-fifth Conference on Neural Information Processing Systems Datasets and Benchmarks Track (Round 2)*, 2021. URL <https://openreview.net/forum?id=wCu6T5xFjeJ>.

Torregrossa, F., Claveau, V., Kooli, N., Gravier, G., and Allesiardo, R. On the correlation of word embedding evaluation metrics. In *LREC 2020-12th Conference on Language Resources and Evaluation*, pp. 4789–4797, 2020.

Viswanathan, K., Gardinazzi, Y., Panerai, G., Cazzaniga, A., and Biagetti, M. The geometry of tokens in internal representations of large language models. *arXiv preprint arXiv:2501.10573*, 2025.

Voorhees, E., Alam, T., Bedrick, S., Demner-Fushman, D., Hersh, W. R., Lo, K., Roberts, K., Soboroff, I., and Wang, L. L. Trec-covid: Constructing a pandemic information retrieval test collection, 2020. URL <https://arxiv.org/abs/2005.04474>.

Wachsmuth, H., Syed, S., and Stein, B. Retrieval of the best counterargument without prior topic knowledge. In *Proceedings of the 56th Annual Meeting of the Association for Computational Linguistics (Volume 1: Long Papers)*, pp. 241–251, 2018.

Wadden, D., Lin, S., Lo, K., Wang, L. L., van Zuylen, M., Cohan, A., and Hajishirzi, H. Fact or fiction: Verifying scientific claims, 2020. URL <https://arxiv.org/abs/2004.14974>.

Wang, B., Wang, A., Chen, F., Wang, Y., and Kuo, C.-C. J. Evaluating word embedding models: Methods and experimental results. *APSIPA transactions on signal and information processing*, 8:e19, 2019.

Wang, L., Yang, N., Huang, X., Jiao, B., Yang, L., Jiang, D., Majumder, R., and Wei, F. Text embeddings by weakly-supervised contrastive pre-training. *arXiv preprint arXiv:2212.03533*, 2022.

Wang, L., Yang, N., Huang, X., Yang, L., Majumder, R., and Wei, F. Multilingual e5 text embeddings: A technical report. *arXiv preprint arXiv:2402.05672*, 2024.

Wang, T. and Isola, P. Understanding contrastive representation learning through alignment and uniformity on the hypersphere. In *International conference on machine learning*, pp. 9929–9939. PMLR, 2020.

Wang, W., Wei, F., Dong, L., Bao, H., Yang, N., and Zhou, M. Minilm: Deep self-attention distillation for task-agnostic compression of pre-trained transformers, 2020. URL <https://arxiv.org/abs/2002.10957>.

Weller, O., Boratko, M., Naim, I., and Lee, J. On the theoretical limitations of embedding-based retrieval. *arXiv preprint arXiv:2508.21038*, 2025.

Wilkie, C. and Azzopardi, L. Relating retrievability, performance and length. In *Proceedings of the 36th international ACM SIGIR conference on Research and development in information retrieval*, pp. 937–940, 2013.

Wilkie, C. and Azzopardi, L. Best and fairest: An empirical analysis of retrieval system bias. In *European Conference on Information Retrieval*, pp. 13–25. Springer, 2014a.

Wilkie, C. and Azzopardi, L. Efficiently estimating retrievability bias. In *European Conference on Information Retrieval*, pp. 720–726. Springer, 2014b.

Willerton, S. Spread: a measure of the size of metric spaces. *International Journal of Computational Geometry & Applications*, 25(03):207–225, 2015.

Wolf, T., Debut, L., Sanh, V., Chaumond, J., Delangue, C., Moi, A., Cistac, P., Rault, T., Louf, R., Funtowicz, M., Davison, J., Shleifer, S., von Platen, P., Ma, C., Jernite, Y., Plu, J., Xu, C., Scao, T. L., Gugger, S., Drame, M., Lhoest, Q., and Rush, A. M. Huggingface’s transformers: State-of-the-art natural language processing, 2020. URL <https://arxiv.org/abs/1910.03771>.

Xiao, S., Liu, Z., Zhang, P., and Muennighoff, N. C-pack: Packaged resources to advance general chinese embedding, 2023.

Xiong, L., Xiong, C., Li, Y., Tang, K.-F., Liu, J., Bennett, P., Ahmed, J., and Overwijk, A. Approximate nearest neighbor negative contrastive learning for dense text retrieval. *arXiv preprint arXiv:2007.00808*, 2020.

Zhang, D., Li, J., Zeng, Z., and Wang, F. Jasper and stella: distillation of sota embedding models, 2025a. URL <https://arxiv.org/abs/2412.19048>.

Zhang, Y., Li, M., Long, D., Zhang, X., Lin, H., Yang, B., Xie, P., Yang, A., Liu, D., Lin, J., Huang, F., and Zhou, Y.

J. Qwen3 embedding: Advancing text embedding and reranking through foundation models. *arXiv preprint arXiv:2506.05176*, 2025b.

Zhao, W. X., Liu, J., Ren, R., and Wen, J.-R. Dense text retrieval based on pretrained language models: A survey. *ACM Transactions on Information Systems*, 42(4):1–60, 2024.

A. Computation of individual topological descriptors

A.1. Persistent Homology Statistics

Let $\{(b_i, d_i)\}_{i=1}^N$ be the birth-death pairs of a Vietoris Rips filtration. We summarize the persistence diagram using:

$$\text{mean lifetime} = \frac{1}{N} \sum_i (d_i - b_i), \quad \text{mean midlife} = \frac{1}{N} \sum_i \frac{b_i + d_i}{2}$$

We use the Python library ripser (Bauer, 2021) for all Persistent Homology computations.

A.2. Persistence Entropy

Let $\ell_i = d_i - b_i$ be the lifetimes and $p_i = \ell_i / \sum_j \ell_j$ the normalized lifetimes. We quantify the complexity of the persistence diagram using the Shannon entropy of the normalized lifetimes:

$$H = - \sum_i p_i \log p_i.$$

A.3. Persistent Homology Dimension

Let X be a bounded subset of a metric space and define the α -weighted sum of the length of persistence intervals, given by their birth b and death d times as:

$$E_i^\alpha = \sum_{(b,d) \in PH_i(x)} (d - b)^\alpha$$

Then dim_i^{PH} for the Vietoris-Rips complex of X corresponds to the smallest α for which E_i^α is uniformly bounded for all subsets of X :

$$dim_i^{PH}(X) = \inf\{\alpha : \exists C \text{ s.t. } E_\alpha^i(x) < C \quad \forall x \subset X\}$$

Intuitively, dim_i^{PH} is determined by how the lengths of the PH intervals for increasing sample sizes vary for a specific homological dimension i . Higher values suggest a more complex topology across scales, as the total persistence (sum of lifetimes) grows rapidly with sample size.

A.4. Euler Characteristic

Let β_i be the i^{th} Betti number, counting the number of independent i -dimensional holes (connected components, loops, voids . . .) in X . Then the Euler Characteristic is given by alternating sums of β_i :

$$\chi = \sum_{i=i}^n (-1)^i \beta_i,$$

A.5. TwoNN Dimension

Let $d_{1,i}$ and $d_{2,i}$ be the distances from point x_i to its first and second nearest neighbors and define the ratio $\mu_i = \frac{d_{2,i}}{d_{1,i}}$. The intrinsic dimension d is computed based on the following equation:

$$-\log(1 - F(\mu)) = d \cdot \log(\mu),$$

where $F(\mu)$ is the empirical cumulative distribution function of μ . Fitting the points $(\log \mu, -\log(1 - F(\mu)))$ with a line through the origin yields the estimate of d . We use the Python library scikit-dimension (Bac et al., 2021) for computations.

A.6. PCA Dimension

Let $\lambda_1 \geq \lambda_2 \geq \dots \geq \lambda_d$ be the eigenvalues of the covariance matrix of the dataset. The Fukunaga–Olsen (FO) rule estimates the intrinsic dimension as the number of eigenvalues larger than a fraction α_{FO} of the largest eigenvalue:

$$\hat{m}_{\text{FO}} = \#\{\lambda_j \mid \lambda_j \geq \alpha_{\text{FO}} \cdot \lambda_{\max}\},$$

where $\lambda_{\max} = \max_j \lambda_j$. We use the Python library `scikit-dimension` (Bac et al., 2021) for computations with $\alpha_{\text{FO}} = 0.5$.

A.7. Effective Rank

Given normalized eigenvalues $p_j = \lambda_j / \sum_k \lambda_k$ of the covariance matrix of X , the effective rank is defined as the Shannon entropy, reflecting the effective number of principal components:

$$\text{ER} = \exp \left(- \sum_j p_j \log p_j \right).$$

A.8. Magnitude and Magnitude function

Given a finite metric space $X = \{x_1, \dots, x_n\} \subseteq \mathbb{R}^D$ and the corresponding similarity matrix $\zeta_X(i, j) := \exp(-d(x_i, x_j))$, then for invertible $\zeta_X(i, j)$ the magnitude of X is defined as:

$$\text{Mag}(X) := \sum_{i,j} (\zeta_X^{-1})_{ij}$$

Using a scaling factor $t \in \mathbb{R}^+$, magnitude can be computed for different scales $d_t(x, y) = t \cdot d(x, y)$ yielding the magnitude function:

$$\text{Mag}_X : t \mapsto \text{Mag}(tX)$$

A.9. Magnitude Dimension

As the scaling factor t grows, the following limit characterizes the asymptotic growth rate of the magnitude function:

$$\dim_{\text{Mag}}(X) := \lim_{t \rightarrow \infty} \frac{\log \text{Mag}(tX)}{\log t},$$

For the computation we use the Python library `magnipy` (Limbeck & Simons, 2025).

A.10. Magnitude Area

The area under the magnitude function is defined as:

$$\text{MagArea} = \int_{t_0}^{t_{\text{cut}}} \text{Mag}_X(t) dt.$$

For the computation we use the Python library `magnipy` (Limbeck & Simons, 2025).

A.11. Spread

Given a finite metric space X with metric d , the spread $E_0(X)$ is measuring the size of the metric space by:

$$E_0(X) := \sum_{x \in X} \frac{1}{\sum_{x' \in X} e^{-d(x, x')}}.$$

A.12. Vendi Score

Let $X = \{x_1, \dots, x_n\} \subseteq \mathbb{R}^D$ be a collection of samples and $K \in \mathbb{R}^{n \times n}$ the corresponding similarity (or more generally kernel) matrix. The Vendi Score is defined as the Shannon entropy of the eigenvalues $\lambda_1, \dots, \lambda_k$ of K/n :

$$\text{VS}_k(x_1, \dots, x_n) = \exp \left(- \sum_i \lambda_i \log \lambda_i \right).$$

A.13. Mean Pairwise Similarity

Density-like descriptor computed from pairwise similarities used as average similarity estimate. We use Cosine similarity and Euclidean similarity as kernels k and compute

$$\bar{s} = \frac{1}{n} \sum_i \frac{1}{n} \sum_j k(x_i, x_j).$$

A.14. Uniformity

Let $X = \{x_1, \dots, x_n\} \subseteq \mathbb{R}^D$ be a collection of samples and $G_t : X^d \times X^d \rightarrow \mathbb{R}_+$ the Radial Basis Function kernel, defined as:

$$G_t(u, v) \triangleq e^{-t\|u-v\|_2^2} = e^{2t \cdot u^\top v - 2t}, \quad t > 0,$$

The uniformity metric (Wang & Isola, 2020) is defined as the logarithm of the average pairwise kernel:

$$\mathcal{L}_{\text{uniform}}(f; t) \triangleq \log \mathbb{E}_{\substack{x, y \sim p_{\text{data}}}} [G_t(u, v)] = \log \mathbb{E}_{\substack{x, y \sim p_{\text{data}}}} \left[e^{-t\|f(x)-f(y)\|_2^2} \right], \quad t > 0.$$

A.15. IsoScore

Given a point cloud $X = \{x_1, \dots, x_n\} \subseteq \mathbb{R}^D$ and its transformation onto the first k principal components X^{PCA} . Define the eigenvalues $\hat{\Sigma}_D$ as the normalized diagonal of the covariance matrix of X^{PCA} . Then IsoScore can be summarized using the following equation:

$$\text{IsoScore}(X) = \frac{n \left(\left(n - \|\hat{\Sigma}_D - \mathbf{1}\|/\sqrt{2(n-\sqrt{n})} \right)^2 (n-\sqrt{n})^2/n^2 \right) - 1}{n-1}$$

A.16. Silhouette Score

For a set of points $X = \{x_1, \dots, x_n\} \subseteq \mathbb{R}^D$ we can measure how well points match their assigned clusters. For point i , let a_i be the mean intra-cluster distance and b_i the mean distance to the nearest other cluster. The Silhouette Score is defined as:

$$s_i = \frac{b_i - a_i}{\max(a_i, b_i)}, \quad \text{Silhouette} = \frac{1}{n} \sum_{i=1}^n s_i.$$

We apply the k -means algorithm to partition the embedding spaces into clusters. To identify the optimal number of clusters, we evaluate

$$k \in \{3, 5, 10, 20, 50, 100\}$$

and compute the corresponding Silhouette Scores. The value of k that maximizes the Silhouette Score is selected and subsequently used as the metric for characterizing the embedding space.

B. Scaling analysis

We perform an empirical scaling analysis across all descriptors to identify an appropriate sample size. This analysis accounts for heterogeneous convergence properties and the varying computational costs associated with the descriptors.

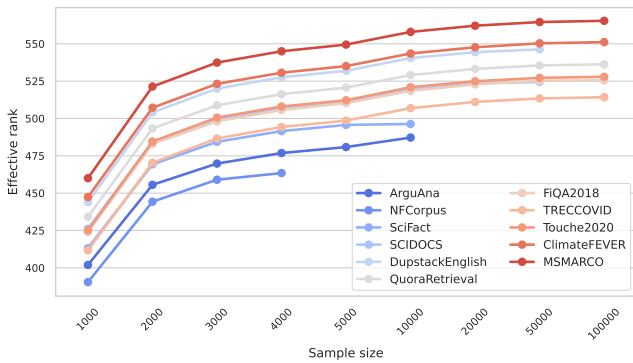


Figure 7. Convergence of the effective rank.

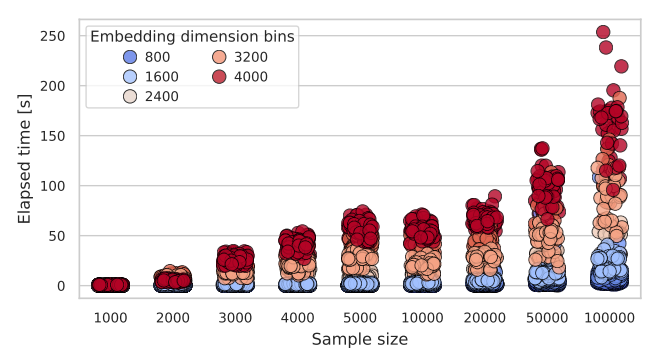


Figure 8. Time complexity of effective rank.

B.1. Convergence

First, we investigate the stability of the measures with increasing sample size, to ensure that the signatures are robust. We found that the metrics react very differently to adjusting the number of samples, for example magnitude area is increasing with sample size, while pairwise distances are converging quickly. An example of this analysis for all datasets is provided in Figure 7, which shows that the measure effective rank starts to converge after 10000 samples. This implies, as some datasets have a lower number of documents, some measures might not fully converge. Additionally, Figure 7 highlights that the absolute values can vary across datasets, while the general convergence pattern is consistent.

B.2. Computational complexity

In addition, we also analyzed the computation time in seconds for each sample size, as shown in Figure 8 for effective rank. We observe that the embedding dimension has a strong influence on the computation time for most descriptors, as higher dimensions lead to more expensive computations. Based on these results, we choose the sample sizes as a balance between computational efficiency and descriptor robustness.

C. Disentangling dataset and model contributions

We observe a variation in descriptor behavior: some characterize the dataset, while others serve as markers of the embedding model itself. For instance, Figure 9 shows a clear anisotropy pattern across models, while the values of different datasets show only little variance for a specific model. This indicates, that this descriptor is suitable for distinguishing between models, but not between datasets. In contrast, Figure 10 shows that intrinsic dimension measured through TwoNN appears to be a property of datasets rather than models, showing significant variance across datasets. These findings have important implications for our normalization scheme. As we normalize the UTS vectors across datasets, we thereby also remove the variability in some descriptors, causing them to be less discriminative. As we are mostly interested in the effects of embedding models, this choice is consistent with our objective of highlighting model-related properties rather than dataset-driven effects.

D. Correlation analysis

We perform a correlation analysis and aggregate the pairwise correlations within each dataset among all used descriptors and additional properties such as the number of model layers and the embedding dimension. Figure 11 shows the mean correlation and variance between datasets, organized using hierarchical linkage clustering. We observe that IsoScore is highly correlated with embedding dimension and effective rank, indicating that larger embedding dimensions lead to more isotropic spaces. Given that persistent homology descriptors emerge from pairwise distances, we find that they are highly correlated with the pairwise similarity descriptor. Finally, most of the intrinsic dimension estimators are correlated with each other, indicating that they capture similar aspects of the data. These correlations allow to select a subset of descriptors that are less expensive to compute, while still capturing the overall topology.

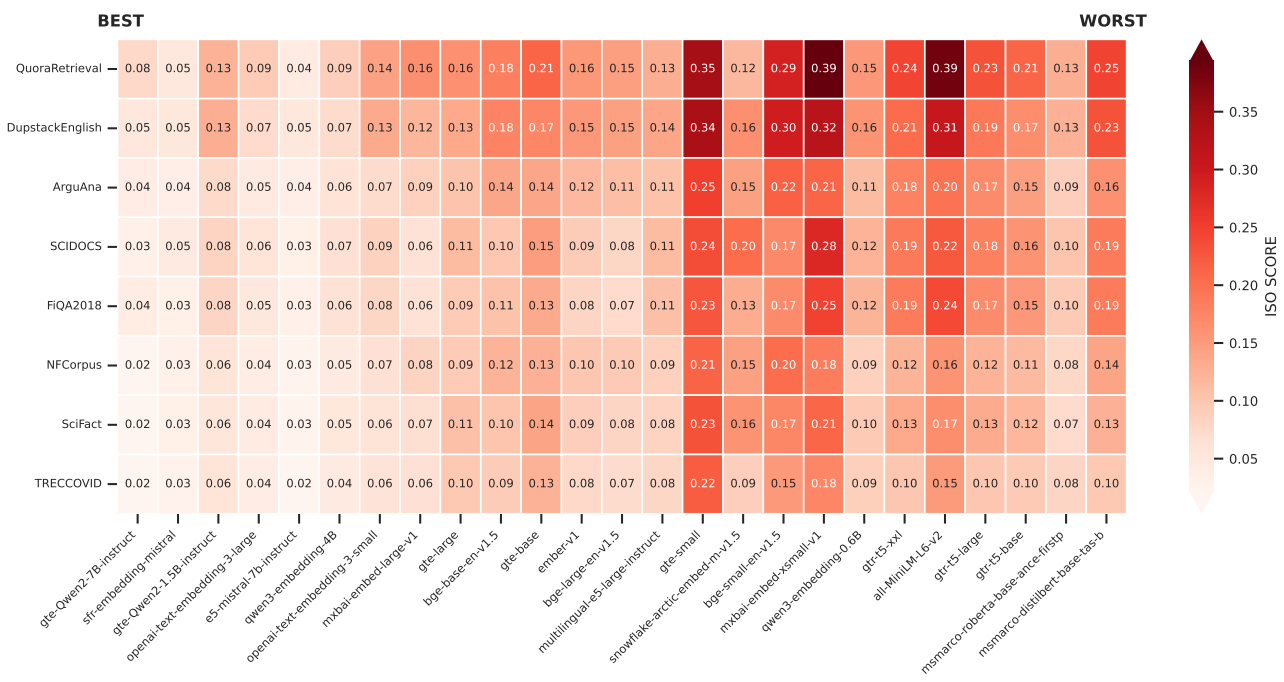


Figure 9. IsoScore of embedding spaces by different models and datasets sorted by MTEB score.



Figure 10. TwoNN dimension of embedding spaces by different models and datasets sorted by MTEB score.

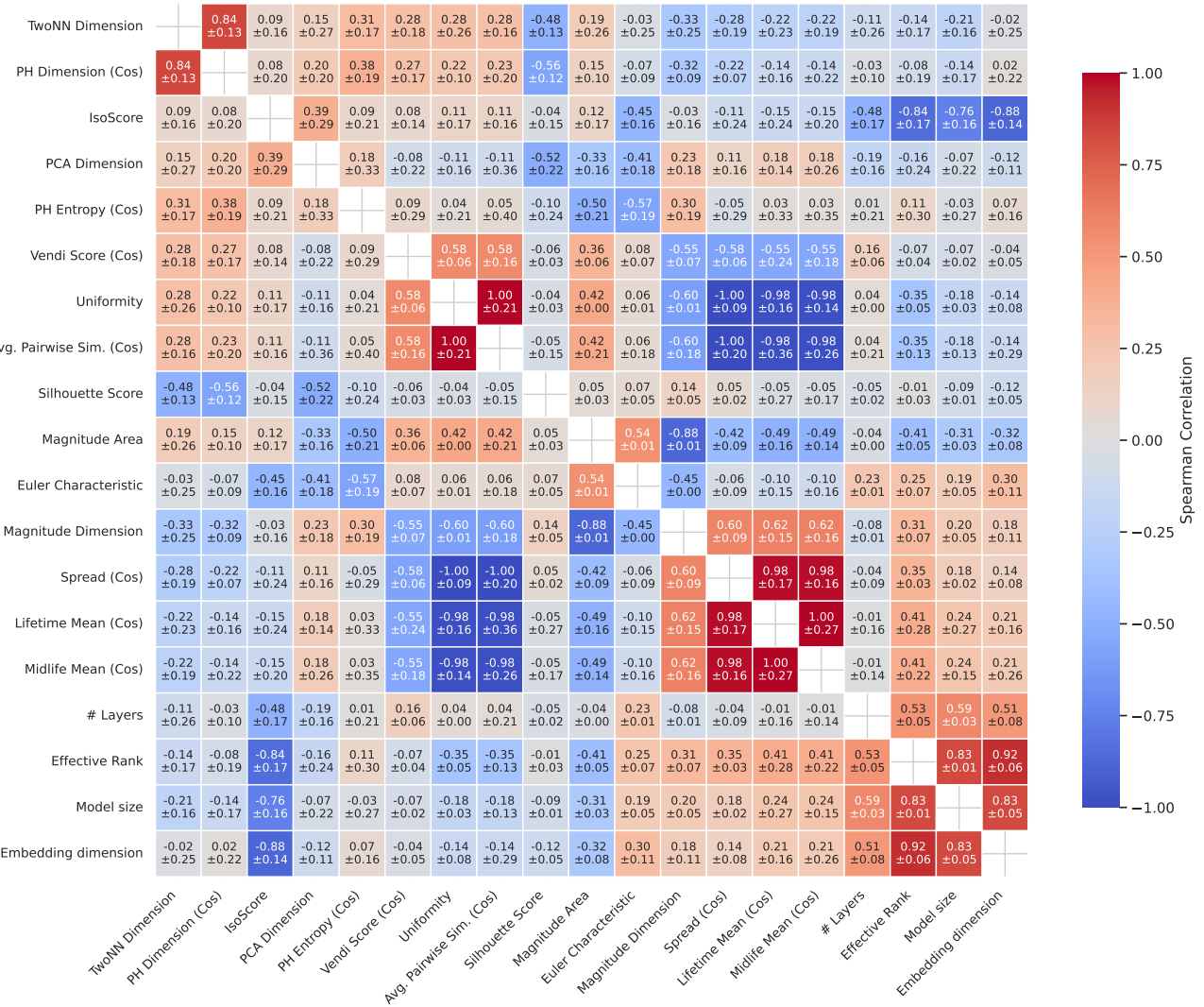


Figure 11. Average correlations of topological descriptors and model properties.

E. Representational similarity analysis

E.1. Centered Kernel Alignment

We compute the Centered Kernel Alignment between all embedding models and datasets and aggregate the average alignment as shown in Figure 12. We find a similar pattern as with our UTS-based similarity measure, emphasizing that the model architecture and training data play a significant role in the alignment of embedding model representations.

E.2. Model size

In addition, we group models into the categories small, medium and large using the parameter count thresholds of $< 0.5B$, $0.5 - 3B$ and $> 3B$ parameters, respectively. By computing UTS similarity, we find that models of the same size are more similar to each other than to models of different sizes. Furthermore, the topologies of large and small models are most different, which can be explained by the dissimilar transformer architectures.

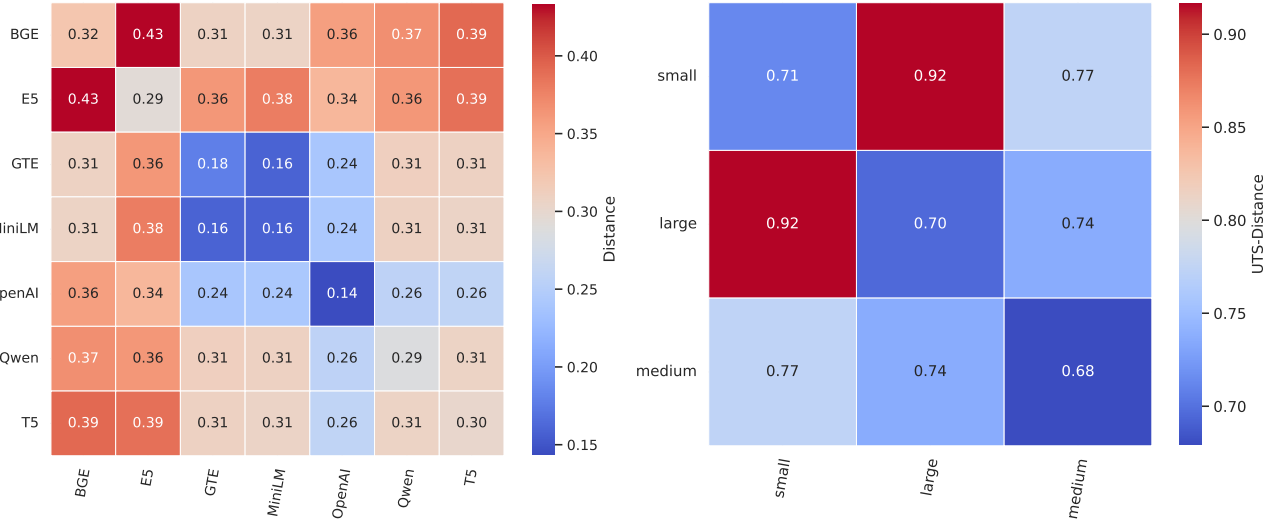


Figure 12. Centered Kernel Alignment between model families.

Figure 13. UTS-based similarity of different model sizes.

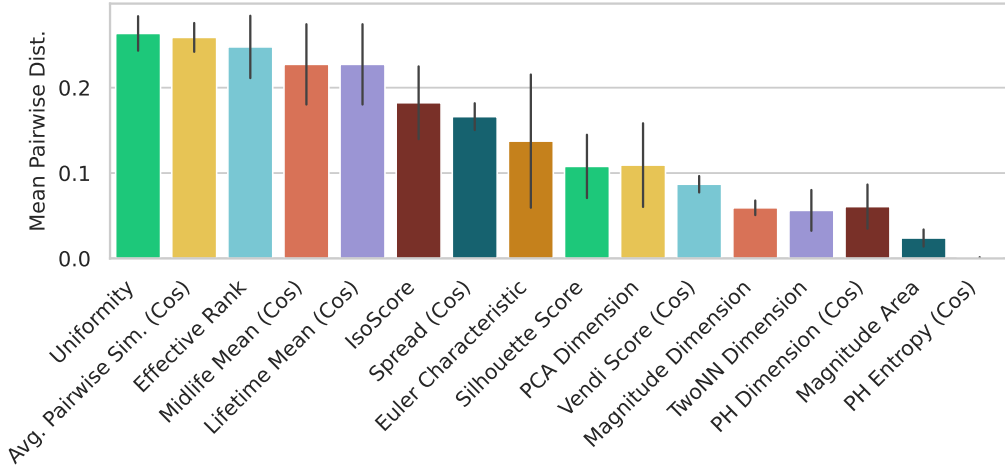


Figure 14. Average distance of UTS components across all models.

E.3. Interpretability of similarity

Our UTS approach enables the interpretability of representational similarity by inspecting the topological drivers that make representations converge. On one hand, we can determine the most discriminative features across all models, as summarized by Figure 14. We find that representations mostly converge due to their density (measured by uniformity and pairwise similarities) as well as their dimensionality (measured by IsoScore and effective rank). Furthermore, similarity is partially driven by the clustering of the embedding spaces. Alongside global interpretations, our framework highlights similarities across embedding spaces by analyzing pairwise comparisons, for example, showing that one space is denser while another is more isotropic. In the context of the Platonic Representation Hypothesis, we specifically find that each model family has different drivers for representational alignment. For instance, Qwen models have a significantly higher effective rank than all other models, while the Clustering coefficient is most discriminative for Gemini models.

F. Influence of dimensionality on retrieval performance

As shown in Figure 15, the effective rank exhibits consistently strong correlations with retrieval performance metrics, such as Recall@20. To visualize this relationship, we encode the embedding model size by marker size and observe that larger models generally correspond to higher effective ranks. This observation aligns with the well known trend that model scale correlates with performance. However, in our setting, a plausible confounding factor is the embedding dimension, which has been shown to play a critical role in retrieval systems (Weller et al., 2025). Indeed, our correlation analysis demonstrates that effective rank is itself highly correlated with the embedding dimension, suggesting that the observed relationship between model size and effective rank is largely attributed to this relationship.

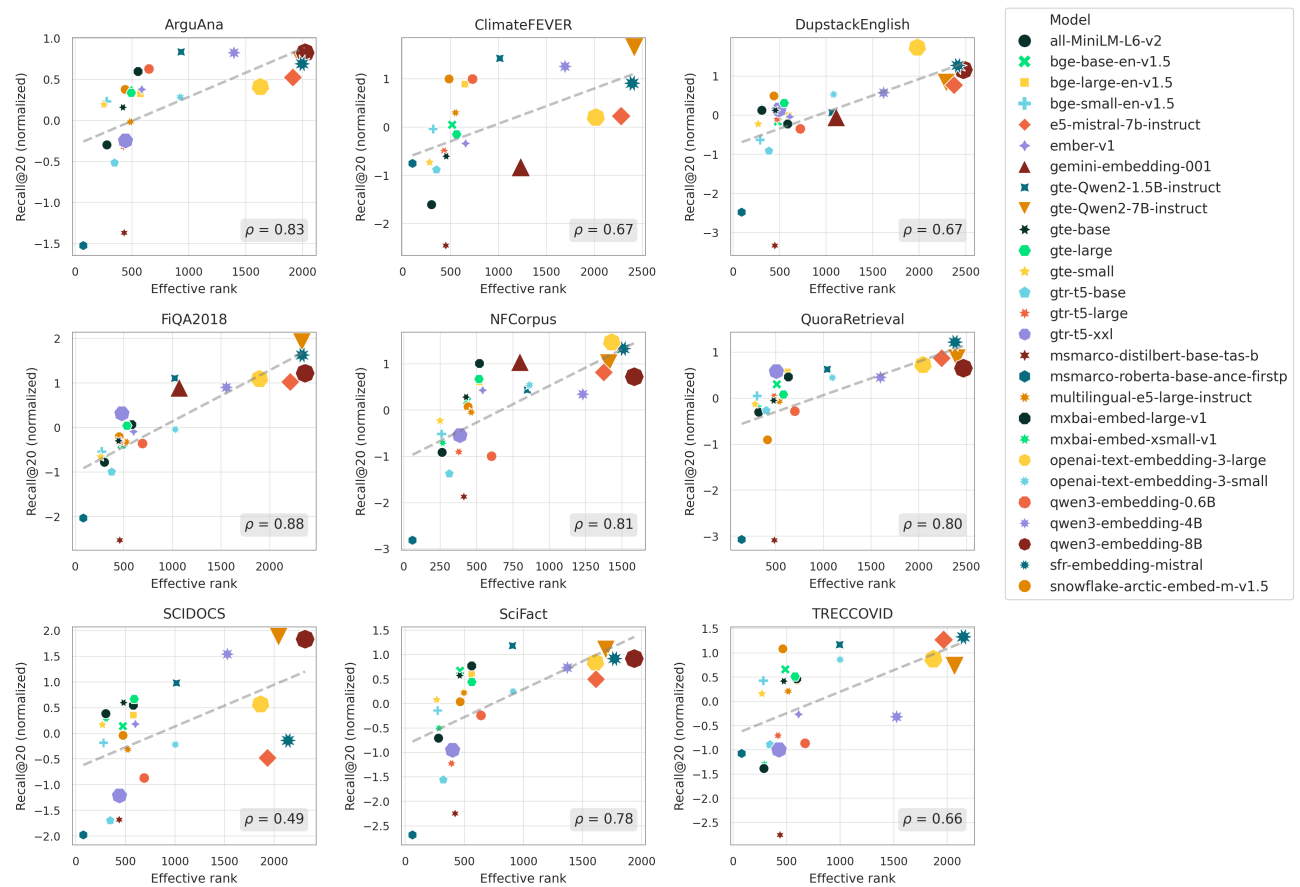


Figure 15. Relationship between normalized Recall@20 and effective rank for different datasets.

G. Predictive analysis

We train classifiers to predict the model architecture (encoder vs. decoder) and the activation function (GELU, ReLU, SiLU) used in unseen embedding spaces. We find that both properties can be predicted with a higher balanced accuracy than the baseline, as summarized in Table 4. For architecture, the binary classification appears to be an easy task, driven by the large difference in embedding dimension between encoder and decoder models. Therefore, we again control for embedding dimension but find that there are too few models of different architectures with the same embedding dimension. For the activation functions, we find a similar pattern suggesting that the same architecture mostly uses the same activation function. Despite this, we are able to predict the architecture used in an embedding spaces with a balanced accuracy of 0.97 ± 0.02 , compared to a baseline of 0.65, and the activation function with a balanced accuracy of 0.67 ± 0.05 , compared to a baseline of 0.53. These results suggest that UTS capture model-specific details encoded in the global topology of the embedding space, motivating further research into understanding how specific architectural choices affect the geometry of embedding spaces, similar to recent work on LayerNorm (Gupta et al., 2024).

We also analyze the effectiveness of the PCA-transformed signature vectors using only the first 5 principal components as features. We find that the average accuracies are slightly lower with 0.39 for predicting the model, 0.45 for predicting model family. This suggests that highly correlated attributes might still complement each other in prediction tasks. In the case of retrieval performance prediction, we achieve comparable results to the full UTS vectors. This can be explained by the large influence of properties related to the embedding dimension, which are captured by the first principal component.

H. Signature clustering analysis

We apply UMAP to the signature vectors of all models, seeds and datasets shown in Figure 16. We encode the model family by different markers, the retrieval performance (normalized Recall@100) by colors and the model size by the size of the points. First, we find that models cluster by model family, which is in line with our previous findings. Moreover, proprietary models developed by OpenAI cluster within the same region as decoder-based models (such as Qwen and E5), highlighting the potential to infer architectural characteristics from our holistic signatures. We also observe a general clustering by model size, which correlates with architecture, given that larger models are typically decoder-based. Finally, we find that sub-clusters correspond to retrieval performance, suggesting that embedding spaces with comparable topology yield similar retrieval outcomes.

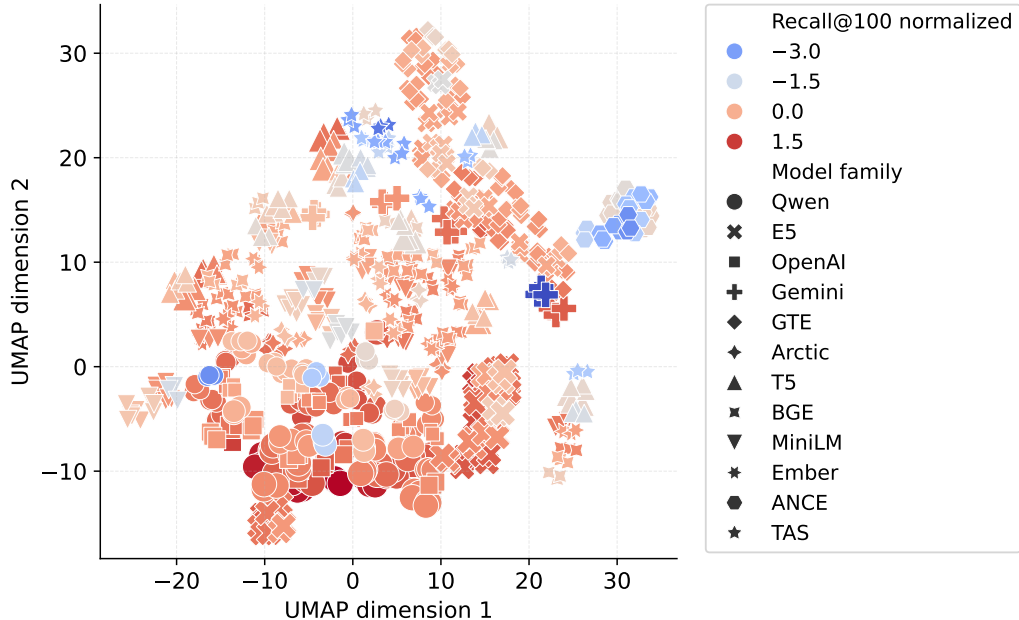


Figure 16. Clustering of Unified Topological Signatures and their normalized Recall@100.

I. Global retrievability analysis

We study the Gini coefficient of the top-100 retrievability distribution to assess the overall bias in a dense retrieval system. As displayed in Figure 17, the retrieval datasets differ in bias strength, which is related to the collection size. Given a fixed query distribution, we observe that that decoder-based models, on average, exhibit a larger bias across most datasets. This implies that they return certain documents more frequently than others. A key difference between the decoder and encoder models used in our experiments is their embedding dimension. We hypothesize, that these effects can be explained by the dimensionality affecting the similarity computation. This is a possible connection to previous studies that have analyzed the influence of dimensionality on retrieval (Reimers & Gurevych, 2021). These findings suggest that not only retrieval performance is associated with embedding dimensionality, but also retrieval bias.

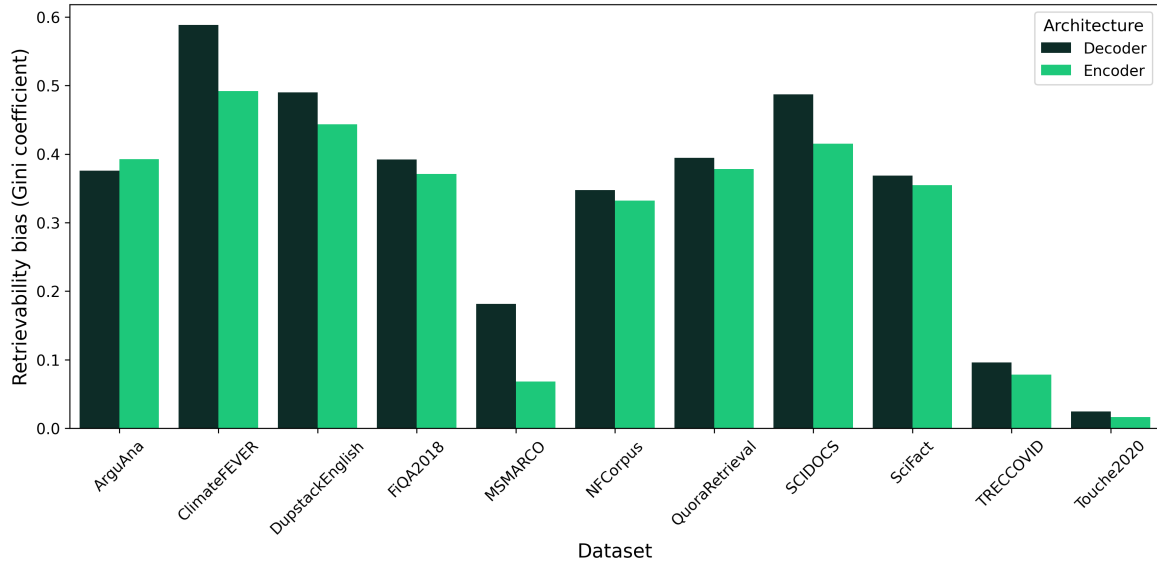


Figure 17. Retrievability bias of encoder and decoder models on different datasets.

J. Local retrievability analysis

J.1. Predictions with raw embeddings

As our results have shown, the topological signatures reveal significant differences between retrievable and non-retrievable documents. We investigate whether such separations exist in the raw embedding space, as this would eliminate the need of computing signatures. For this, we use UMAP to visualize the raw embedding space and compare it with the UTS space, color-coding the retrievability of documents. As Figures 18–23 show, the UTS space provides a much clearer separation than the raw embedding space, motivating our approach. These findings are supported by the lower accuracy of the baseline prediction model, as reported in the results section. Finally, even if the raw embedding space shows a partial separation (e.g. Figure 22), such trends do not extrapolate well to embedding spaces of other datasets, unlike our proposed UTS vectors.

J.2. Characteristics of retrievable documents

To gain deeper insight into the topological features that influence document retrievability, we analyze the differences between retrievable and non-retrievable clusters. For this, we select 10 data points from each of the clusters and compare their topological signatures. As Figure 24 shows, the local topology has distinct values for several descriptors, highlighting the importance of our unified approach. Further, we find that the largest differences lie in properties related to the density of the embedding space, suggesting that less retrievable documents lie in isolated regions. Beyond density, we also find that the neighborhood of highly retrievable documents has lower intrinsic dimensions. These observations are reinforced by the feature importance analysis of the prediction model as summarized by Figure 25.

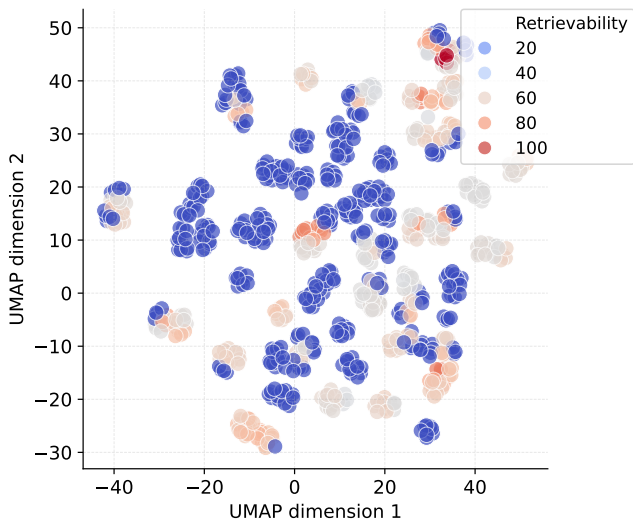


Figure 18. ArguAna raw embeddings for text-embedding-3-large.

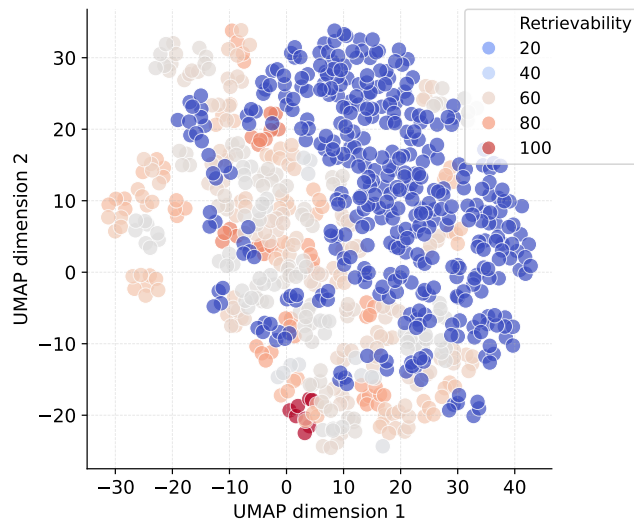


Figure 19. ArguAna local UTS for text-embedding-3-large.

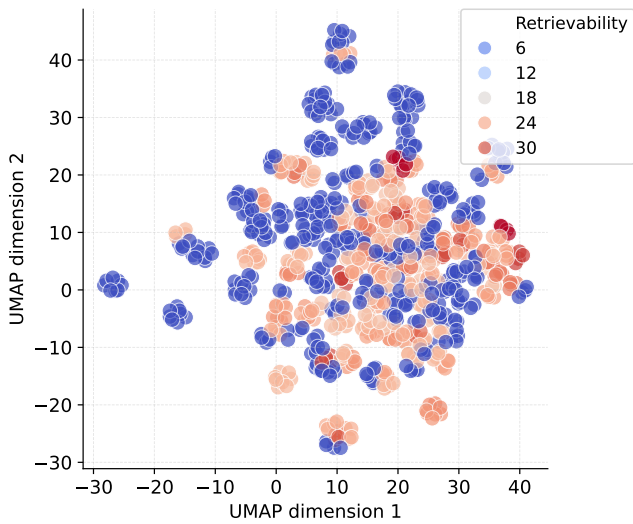


Figure 20. NFCorpus raw embeddings for e5-mistral-7b-instruct.

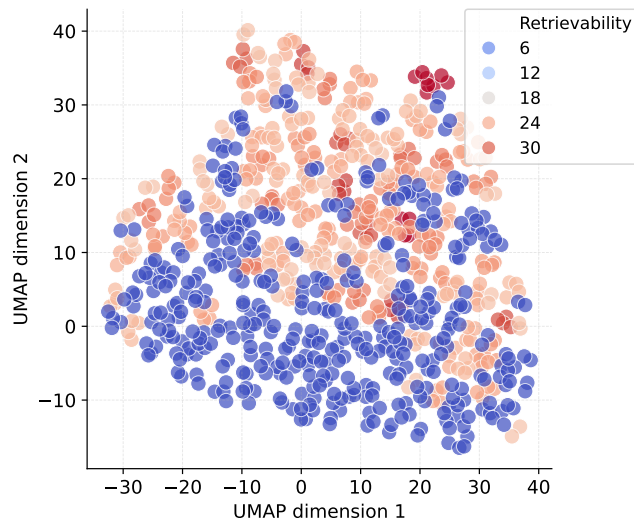
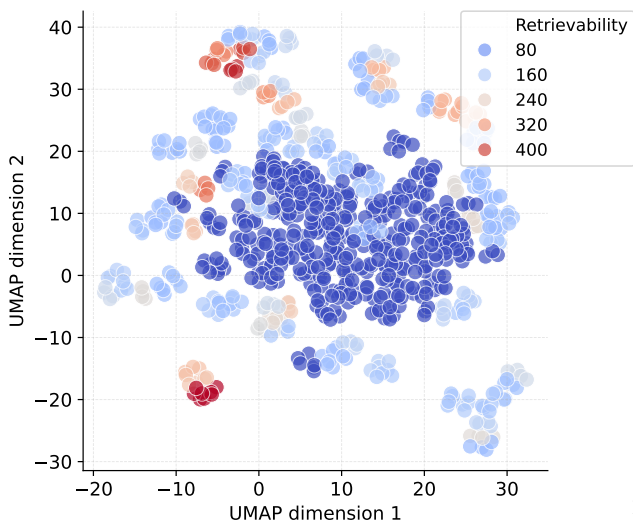


Figure 21. NFCorpus local UTS for e5-mistral-7b-instruct.



24

Figure 22. Quora raw embeddings for multilingual-e5-large.

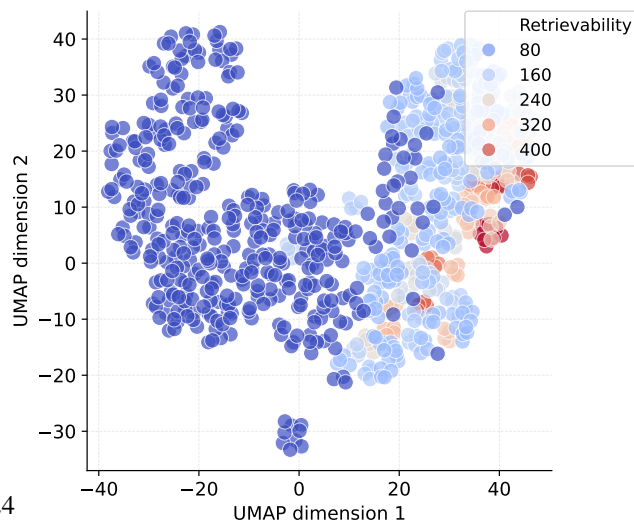


Figure 23. Quora local UTS for multilingual-e5-large.

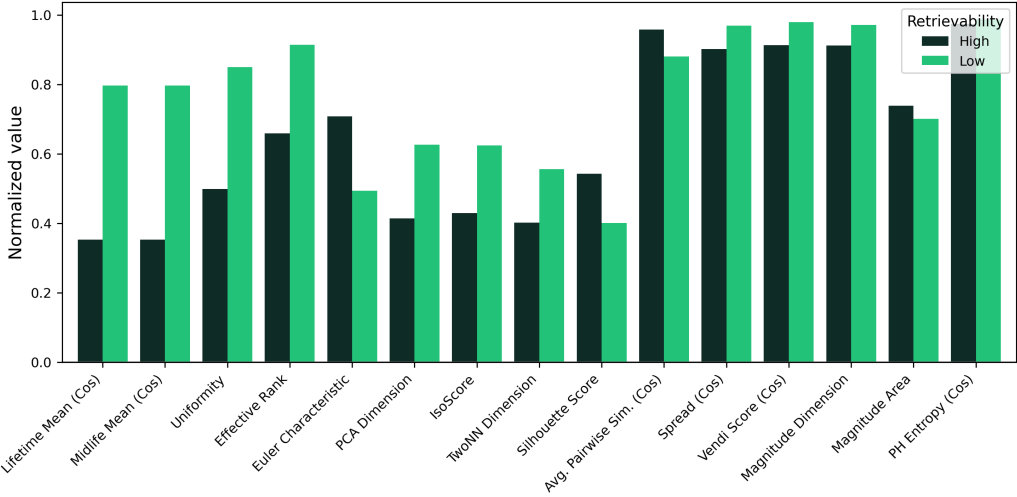


Figure 24. Differences between clusters of highly retrievable and non-retrievable documents for QuoraRetrieval dataset.

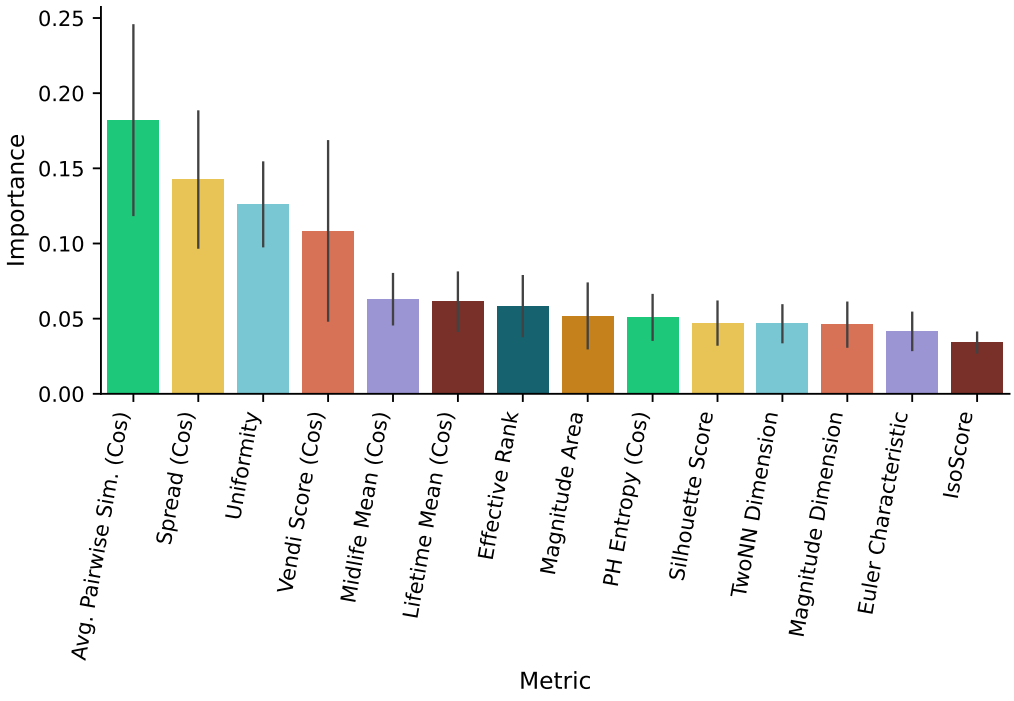


Figure 25. Feature importance for predicting retrievability.

J.3. Retrievability of embedding models

We investigate whether embeddings differ in their ability to predict document retrievability. For this, we fit prediction models for each embedding model and evaluate the accuracy using group cross-validation. As Figure 26 shows, there are large differences in the accuracy between different models, with gemini-embedding-001 achieving the best results. This suggests that the structural characteristics of local topologies vary across models, motivating further exploration of retrievability.

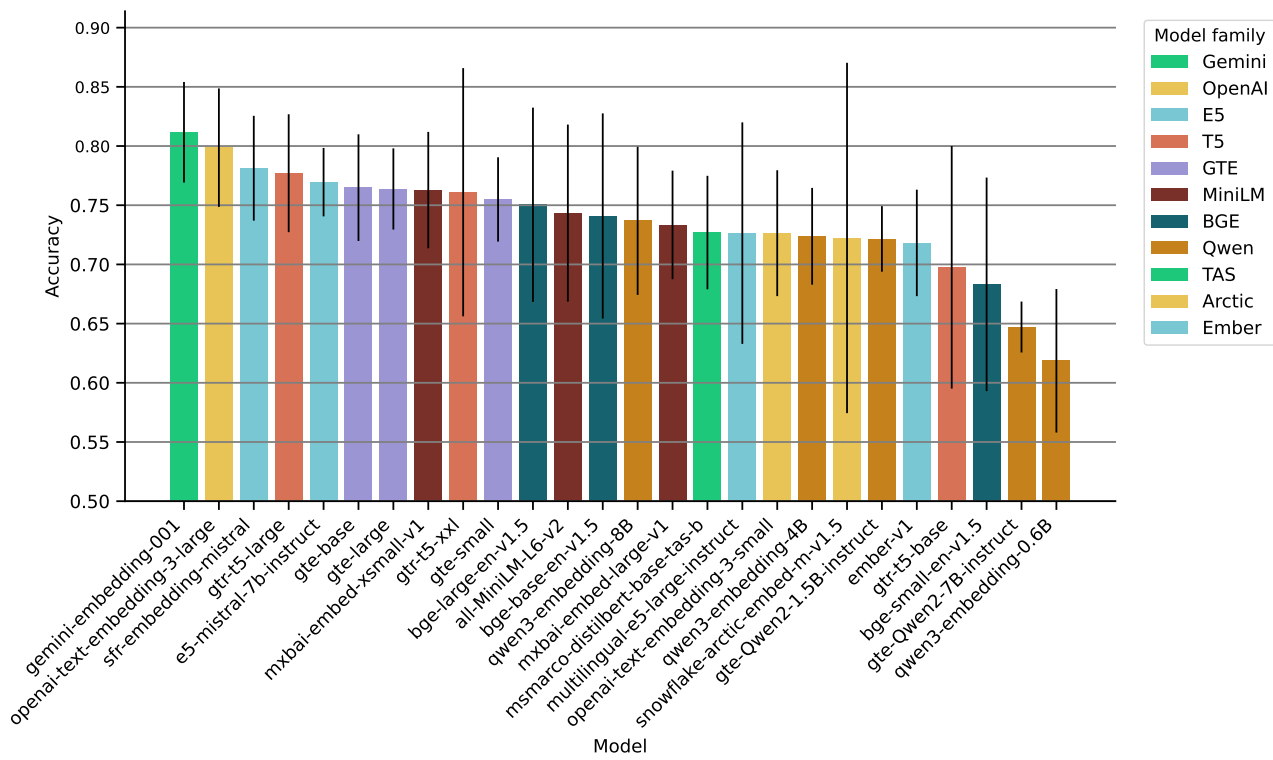


Figure 26. Comparison of accuracies by different models for predicting retrievability.